

# MUSE Analysis of Gas around Galaxies (MAGG) - V: Linking ionized gas traced by C IV and Si IV absorbers to Ly $\alpha$ emitting galaxies at $z \approx 3.0 - 4.5$ .

Marta Galbiati,<sup>1</sup>\* Michele Fumagalli,<sup>1,2</sup>† Matteo Fossati,<sup>1,3</sup> Emma K. Lofthouse,<sup>1,3</sup> Rajeshwari Dutta,<sup>1,3</sup> J. Xavier. Prochaska,<sup>4,5</sup> Michael T. Murphy,<sup>6</sup> Sebastiano Cantalupo<sup>1</sup>

<sup>1</sup>Dipartimento di Fisica G. Occhialini, Università degli Studi di Milano-Bicocca, Piazza della Scienza 3, 20126 Milano, Italy

<sup>2</sup>INAF - Osservatorio Astronomico di Trieste, via G. B. Tiepolo 11, 34143 Trieste, Italy

<sup>3</sup>INAF - Osservatorio Astronomico di Brera, via Brera 28, 21021 Milano, Italy

<sup>4</sup>Department of Astronomy and Astrophysics, University of California, Santa Cruz, CA 95064, USA

<sup>5</sup>Kavli Institute for the Physics and Mathematics of the Universe, 5-1-5 Kashiwanoha, Kashiwa 277-8583, Japan

<sup>6</sup>Centre for Astrophysics and Supercomputing, Swinburne University of Technology, Hawthorn, Victoria 3122, Australia

## ABSTRACT

We use 28 quasar fields with high-resolution (HIRES and UVES) spectroscopy from the MUSE Analysis of Gas Around Galaxies survey to study the connection between Ly $\alpha$  emitters (LAEs) and metal-enriched ionized gas traced by C IV in absorption at redshift  $z \approx 3 - 4$ . In a sample of 220 C IV absorbers, we identify 143 LAEs connected to C IV gas within a line-of-sight separation  $\pm 500 \text{ km s}^{-1}$ , equal to a detection rate of  $36 \pm 5$  per cent once we account for multiple LAEs connected to the same C IV absorber. The luminosity function of LAEs associated with C IV absorbers shows a  $\approx 2.4$  higher normalization factor compared to the field. C IV with higher equivalent width and velocity width are associated with brighter LAEs or multiple galaxies, while weaker systems are less often identified near LAEs. The covering fraction in groups is up to  $\approx 3$  times larger than for isolated galaxies. Compared to the correlation between optically-thick H I absorbers and LAEs, C IV systems are twice less likely to be found near LAEs especially at lower equivalent width. Similar results are found using Si IV as tracer of ionized gas. We propose three components to model the gas environment of LAEs: i) the circumgalactic medium of galaxies, accounting for the strongest correlations between absorption and emission; ii) overdense gas filaments connecting galaxies, driving the excess of LAEs at a few times the virial radius and the modulation of the luminosity and cross-correlation functions for strong absorbers; iii) an enriched and more diffuse medium, accounting for weaker C IV absorbers farther from galaxies.

**Key words:** galaxies: haloes – galaxies: high-redshift – intergalactic medium – quasars: absorption lines – galaxies: formation – galaxies: evolution – galaxies: groups

## 1 INTRODUCTION

Based on our current understanding of the onset of the first episodes of star formation in halos hosting population III stars, heavy elements are produced in a primordial Universe. Due to the massive nature of these first stars, the newly-produced metals are not always retained in compact objects, but are ejected into the interstellar medium (ISM) and, owing to energetic events, also in the circumgalactic medium (CGM) and the intergalactic medium (IGM), contributing to the early enrichment of the Universe (e.g. Scannapieco et al. 2002; Schneider et al. 2002; Maio et al. 2011; Wise et al. 2012). Likewise, stellar winds and supernova explosions associated with the formation of the subsequent generations of stars in galaxies are believed to be the source of a substantial fraction of the heavy elements we observe today near and outside galaxies (e.g. Aguirre et al. 2001; Oppenheimer & Davé 2006; Shen et al. 2013), with mechanisms like winds from active galactic nuclei, gravitational interactions or ram-pressure stripping accounting for an additional fraction of the metals found

outside galaxies (e.g. Fossati et al. 2016; Hafen et al. 2019). Due to the tight correspondence between the production of metals by stars and the subsequent ejection into the CGM and IGM, the study of the chemical enrichment of the more diffuse gas outside and around galaxies as a function of time is a powerful tool to complement our view of the star formation history in galaxies (e.g. Bouché et al. 2006; Rafelski et al. 2014; Madau & Dickinson 2014; Fumagalli et al. 2016), and a fundamental step for developing complete chemical evolution models (e.g. Tremonti et al. 2004; Finlator & Davé 2008; Welsh et al. 2019).

The most effective way to map the chemical enrichment of the low-density IGM and CGM is, at present, the study of hydrogen and metal absorption lines imprinted on the spectra of background sources, such as quasars. Compilations of high-resolution spectra, as well as moderate-to-low resolution spectroscopy in larger surveys, paint a view of a widespread metal enrichment of the Universe at least for gas around or above the mean density (e.g. Schaye et al. 2003; Simcoe et al. 2004), with only a few rare exceptions of unpolluted regions observed below  $z \lesssim 4.5$  (e.g. Fumagalli et al. 2011; Robert et al. 2019).

The analysis of the C IV doublet with its two strong transitions at

\* E-mail: m.galbiati29@campus.unimib.it

† E-mail: michele.fumagalli@unimib.it

1548.195Å and 1550.770Å and a characteristic ratio of the optical depth for unsaturated lines equal to two (given by the ratio of the corresponding oscillator strengths) has been particularly effective for this type of study, enabling the identification of this ion also in moderate signal-to-noise and low resolution data. In particular, recent searches of C iv doublets in Sloan Digital Sky Survey quasar spectra by [Cooksey et al. \(2013\)](#) and in quasar spectroscopy from the Keck and Very Large Telescope (VLT) archives by [Hasan et al. \(2020\)](#) consistently show a steady increase of the number of C iv absorbers per unit redshift with time. As the observed incidence of C iv is proportional to the comoving number density of C iv bearing systems times their cross section, one can learn about the link between C iv and galaxies in a model-dependent fashion. For instance, assuming that C iv absorbers with equivalent width (EW) > 0.06 Å arise in the CGM of Lyman break galaxies (LBGs), [Cooksey et al. \(2013\)](#) estimated that the observed incidence can be modelled by filling the inner ≈ 50 kpc of LBGs halos with ionized carbon with time. More recently, [Hasan et al. \(2021\)](#) expanded this argument both in mass and redshift, combining C iv absorption statistics with dark matter halos to constrain the link between gas and galaxies.

Leveraging the deployment of echellette spectrographs in the near infrared, [Simcoe et al. \(2011\)](#) have expanded previous efforts to characterise the evolution of C iv in quasar surveys at even higher redshift (see also [Pettini et al. 2003](#); [Songaila 2005](#)), reaching the epoch of reionization at  $z \approx 6$  and confirming the presence of a downturn in the mass density of C iv beyond  $z \approx 5$ . These studies in large samples are complemented by the orthogonal approach followed by [D’Odorico et al. \(2016\)](#) who have obtained an extremely-high  $S/N$  spectrum of a single quasar, measuring the distribution of some of the weakest C iv lines currently detected around column density  $N_{\text{CIV}} = 10^{11.4} \text{ cm}^{-2}$  (see also [Ellison et al. 2000](#)). Their analysis reveals a factor ≈ 2 higher incidence of C iv lines associated with H I than what is expected in LBG halos, implying the presence of metals in IGM filaments or in the CGM of galaxies not selected as LBGs (e.g. at lower mass; see also [Pieri et al. 2006](#); [Hasan et al. 2021](#)).

While absorption line studies currently remain the most powerful approach to trace the entire distribution of the selected ions regardless of the astrophysical environment in which they reside (e.g. IGM, CGM at different halo masses), more direct links between the production sites of heavy elements and their current location requires an explicit correlation between the ions detected in absorption and the surrounding galaxy population traced in emission. Focusing on C iv as a tracer, [Dutta et al. \(2021\)](#) have completed the largest survey to date of galaxies in quasar fields between  $0.5 \lesssim z \lesssim 2$ , finding that C iv is relatively more extended than Mg II around galaxies (see also [Liang & Chen 2014](#); [Schroetter et al. 2021](#)). Further, they reported a higher incidence of C iv around massive and star-forming galaxies (see also [Chen et al. 2001](#); [Bordoloi et al. 2014](#); [Burchett et al. 2016](#)), although this ion appears comparably less sensitive than Mg II with respect to the properties of the galaxies and of the environment. However, in the local Universe, [Burchett et al. \(2016\)](#) have uncovered an environmental dependence, with a higher detection rate in lower-density regions. Moreover, [Schroetter et al. \(2021\)](#) further explored the connection between C iv absorbers and galaxies, finding a non-negligible fraction of instances where ionized gas can be associated to the IGM or undetected low-mass galaxies.

At redshift  $2 \lesssim z \lesssim 3$ , [Adelberger et al. \(2005\)](#) have provided the first clear evidence of an association between strong C iv absorbers and massive (with halo mass  $M_{\text{H}} \approx 10^{12} M_{\odot}$ ) star-forming galaxies (with star formation rate, SFR, ≈ 10–50  $M_{\odot} \text{ yr}^{-1}$ ) selected as LBGs (see also [Crighton et al. 2011](#)), with these types of halos accounting for ≈ 1/3 of all C iv absorbers with EW > 0.4 Å. Their study

has also suggested that galaxies in denser environments are more likely to show C iv in absorption compared to isolated galaxies. The ubiquitous presence of C iv near LBGs is also confirmed by later studies building on the same sample presented by [Adelberger et al. \(2005\)](#), with [Steidel et al. \(2010\)](#) using galaxy pairs to infer that LBGs account for almost 50% of strong (EW > 0.15 Å) C iv systems at  $z \approx 2$  (see also [Turner et al. 2014](#)).

These studies rely on spectroscopic follow-up of relatively-bright continuum-selected galaxies and, especially at  $z > 2$ , focus on the massive end of the galaxy population. For a complete view of the correlation between galaxies and metals, this type of analysis needs to be extended at the low-mass end, and to encompass also passive or highly-obscured galaxies. The serendipitous discovery of a faint Ly $\alpha$  emitting galaxy (LAE) associated with a metal-rich absorption system in an LBG survey by [Crighton et al. \(2015\)](#) provides a clear example of the need to extend this analysis to lower-mass galaxies without relying on continuum selection (see also [Díaz et al. 2015](#)), an approach that is now possible (see e.g. [Fumagalli et al. 2016, 2017](#)) thanks to large integral field spectrographs and in particular the Multi Unit Spectroscopic Explorer (MUSE; [Bacon et al. 2010](#)) at VLT. To this end, the recent  $z \approx 3 - 4$  MUSE observations by [Muzahid et al. \(2021\)](#) have identified 96 LAEs in 8 quasar fields. By correlating these galaxies with C iv absorption, these authors found an elevated C iv optical depth near LAEs similarly to the case of LBGs. They also report evidence of an excess of absorption near LAEs in groups compared to isolated ones. Examples of similar studies extending to higher redshift can also be found in the literature ([Bielby et al. 2020](#); [Díaz et al. 2021](#)).

In this paper, we exploit the larger MUSE Analysis of Gas around Galaxies (MAGG, [Lofthouse et al. 2020](#)) survey to study in detail the correlation between 292 LAEs and 220 C iv absorbers. To verify whether the link between LAEs and ionized gas traced by C iv is specific to the selected transition or general for a ionized gas phase, we also expand our study to the associations between LAEs and Si iv, which is an additional doublet that arises from moderately-ionized gas and it is conveniently accessible in a comparable wavelength range to C iv. MAGG is built on a MUSE Large Programme (ID 197.A-0384; PI Fumagalli) that was explicitly designed to study the link between gas and galaxies at  $z \approx 3 - 4$  by targeting 28 fields with quasars at  $z \approx 3.2 - 4.5$  for which archival high-resolution ( $R \gtrsim 30,000$ ) spectroscopy is available ([Lofthouse et al. 2022](#), hereafter MAGG IV; see also [Dutta et al. 2020](#); [Fossati et al. 2021](#)). The MAGG selection results in a sample of quasars with magnitudes  $m_{\text{r}} \leq 19$  mag and at least one strong hydrogen absorption line system ( $N_{\text{HI}} \geq 10^{17} \text{ cm}^{-2}$ ) at redshift  $z \geq 3.05$ .

The structure of this paper is as follows: in Sect. 2-3 we present an overview of the observations and data analysis, including a description of how the LAEs, C iv and Si iv samples have been assembled. Readers not interested in technical details on data can skip these two sections. In Sect. 4 we turn to the main question of studying in detail the correlation between LAEs and C iv absorbers as a function of galaxy properties and environment, also comparing with the results obtained by relying on Si iv rather than C iv as a tracer of ionized gas. We discuss our main findings and conclusions in Sect. 5-6. Throughout, we assume a flat  $\Lambda$ CDM cosmology with  $H_0 = 67.7 \text{ km s}^{-1} \text{ Mpc}^{-1}$  and  $\Omega_{\text{m}} = 0.307$  ([Planck Collaboration et al. 2016](#)), magnitudes are expressed in the AB system, distances are in physical units unless explicitly stated (for instance when computing the correlation functions), and errors are at  $1\sigma$  confidence level.

## 2 OBSERVATIONS AND DATA REDUCTION

### 2.1 MUSE observations

Each quasar field included in the MAGG survey has been observed with MUSE between period 97 and period 103, for a total on-source observing time of  $\approx 4$  hours per field using the wide field mode with extended wavelength coverage (465 – 930 nm,  $R \approx 2000 - 3500$ ). As part of this survey, we also include archival data from the GTO observations (PI Schaye; Muzahid et al. 2021) that matched the selection criteria of the original MAGG sample (i.e., the presence of  $z > 3$  H I optically-thick absorption systems along the line of sight; see details in table 1 of Lofthouse et al. 2020).

All the observations have been executed on clear nights at airmass  $\leq 1.6$  so that the image quality is better than 0.8 arcsec full width at half maximum (FWHM). Image quality for individual fields can be found in table 1 of Lofthouse et al. 2020. In wide field mode, the MUSE field of view (FoV) is  $\approx 1 \times 1$  arcmin<sup>2</sup>. In our observations, the quasar typically lies at the center of the FoV, enabling deep spectroscopic surveys of regions of  $\approx 500 \times 500$  kpc<sup>2</sup> at redshift  $z \approx 3$ . As documented in the MUSE instrument manual, sensitivity variations across the FoV may arise from small differences in the performance of the MUSE spectrographs, and these are mitigated by including small dithers and instrument rotations of 90 degrees.

The detailed procedure of MUSE data reduction is described by Lofthouse et al. (2020), and only the key steps are summarized here. The raw data are first processed with the ESO MUSE pipeline (Weilbacher et al. 2014, version 2 or greater) which applies bias and flat calibrations, reduces the sky flats, and reconstructs the cube of individual exposures following wavelength calibration. Each individual exposure is then post-processed with the CUBEXTRACTOR package (CUBEx, Cantalupo et al. 2019), which is one of the available tools to improve the quality of the datacubes and mitigate the known imperfections arising after the basic ESO pipeline reduction (see figure 1 in Lofthouse et al. 2020). In particular, the residual differences in the relative illumination of the 24 MUSE IFUs are corrected with the CUBEFIX tool in CUBEx which scans the cube as a function of wavelength to re-align the relative illumination of the IFUs. Next, the CUBESHARP tool (also part of CUBEx) is used to perform local sky subtraction removing the residuals left from the ESO pipeline reduction, by taking into account spatial variations in the line spread function of the instrument. A second iteration using both these tools is then performed masking continuum-detected sources to enable an improved determination of the background. At the end of the reduction process, in order to allow a more accurate identification of possible contaminants, all the single exposures are combined in four final products: an average cube of all the exposures (mean cube), a median cube and two cubes, each containing only one half of all the exposures. These last two products are useful to confirm the detection of sources in two independent datasets.

As fully described by Lofthouse et al. (2020), the uncertainties of each pixel are computed by propagating the detector noise through the whole reduction process. Since the individual pixels are transformed across several steps, including the non-linear interpolation leading to the final data cube, the resulting pixel variance does not accurately reproduce the effective standard deviation of each volumetric pixel. Following the procedure detailed by Fossati et al. (2019), we derive a series of data cubes with accurate estimates of the standard deviation by bootstrapping the pixels in individual exposures in order to compute the noise in each final product.

### 2.2 High-resolution quasar spectroscopy

All the quasars included in the MAGG survey have high-resolution ( $R \gtrsim 30,000$ ) and moderate or high signal-to-noise ( $S/N \gtrsim 10$  per pixel, for details see table 2 of Lofthouse et al. 2020) spectra obtained with the Ultraviolet and Visual Echelle Spectrograph (UVES, Dekker et al. 2000) at the VLT, the High Resolution Echelle Spectrometer (HIRES, Vogt et al. 1994) at Keck, or the Magellan Inamori Kyocera Echelle (MIKE; Bernstein et al. 2003) at the Magellan telescopes. Moderate dispersion spectra from X-SHOOTER (Vernet et al. 2011) at the VLT and Echelle Spectrograph and Imager (ESI, Sheinis et al. 2002) at Keck are also used to extend the observed wavelength range. Details on the reduction procedure for each instrument and a summary of the data available for each quasar are described by Lofthouse et al. (2020) in section 3.1 and listed in their table 2. The main observational information that are summarized therein include: the wavelength range covered by the data, the spectral resolution, and the final signal-to-noise ratio at selected wavelengths.

## 3 DATA ANALYSIS

### 3.1 Catalogue of C iv absorption lines

We visually inspect the high-resolution quasar spectra searching for C iv  $\lambda\lambda$  1548, 1550 resonant doublets, identified through the characteristic rest wavelength separation of 2.575 Å, corresponding to 489 km s<sup>-1</sup>, and the equivalent width ratio 2:1 for  $W_r^{1548} : W_r^{1550}$  in the unsaturated regime. For the sightlines where multiple observations from different instruments are available, we choose to inspect the spectrum with the highest signal-to-noise ratio for each sightline in a specific wavelength range.

The inspection is limited to in the wavelength range lying redward the quasar Ly $\alpha$  forest, so as to exclude wavelengths in which metals are only the minority of the observed transitions and thus hard to detect due to the severe blending. We also exclude small windows that overlap with known strong telluric bands at 6870-6935 Å and 7595-7700 Å since these contaminant lines of the Earth's atmosphere could be more easily misinterpreted as false positives. To obtain the highest possible purity of the sample, we also reject all the candidate C iv doublets that show nonphysical line ratios (i.e., not matching the ratio set by the oscillator strengths) in the range 7180-7295 Å, a further window that is contaminated by the presence of additional weak telluric features. Lastly, we mask a velocity window  $|\Delta v| < 3000$  km s<sup>-1</sup> from the redshift of each quasar to avoid proximity effects. The resulting sample includes 467 candidate absorbers in the redshift range  $z \approx 2 - 4$ . To reduce the subjectivity of human classification performed at this stage, candidates absorbers are vetted by two authors (MG and RD) independently. Since the galaxies targeted in the optical band observed by MUSE lie at  $z > 3$ , we further restricted our sample to the systems above this redshift, for a total of 332 candidate C iv absorbers.

The availability of high resolution spectra, with intrinsic widths of the lines often resolved, allows us to model the absorption lines as Voigt profiles, see Figure 1 for a few examples. Once the spectra are continuum-normalized (see Lofthouse et al. 2020 for the detailed procedure), we fit each candidate doublet with Voigt profiles by running the MC-ALF code (Fossati et al. 2019). Using a Bayesian formalism in which the likelihood is sampled with a nested sampling algorithm and the best model is chosen via the Akaike Information Criterion, this code models the absorption profiles assuming an initial number of components within an interval based on visual inspection of each line (e.g, typically ranging between  $\approx 5 - 10$  Å for most profiles) and

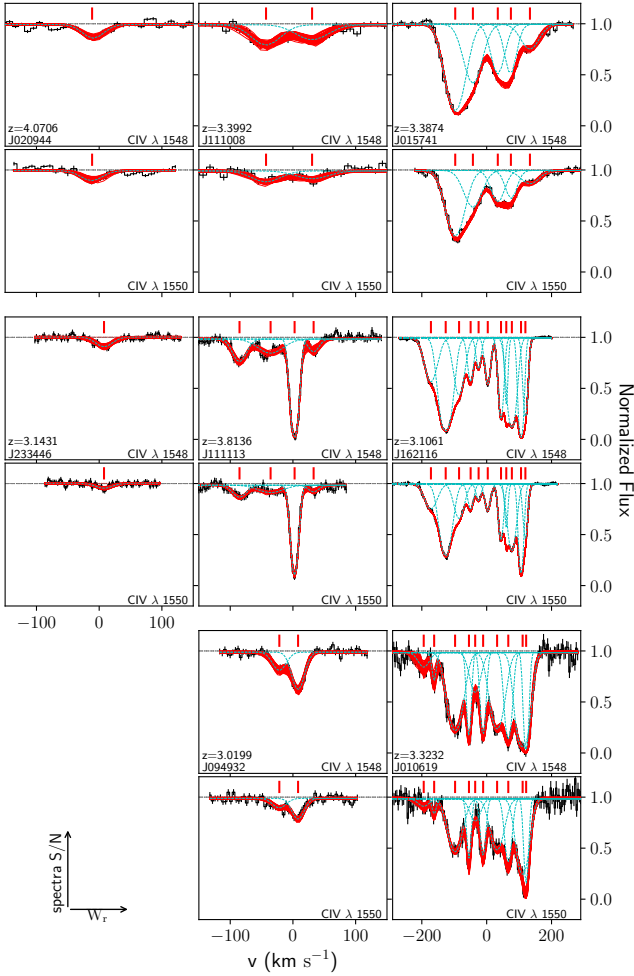


**Figure 1.** Examples of CIV doublet absorption line systems detected in MAGG quasar spectra at different  $S/N$  ( $S/N \leq 20$ ,  $20 < S/N < 40$  and  $S/N \geq 40$ ) and randomly extracted from three bins of CIV equivalent width ( $W_r/\text{\AA} \leq 0.03$ ,  $0.03 < W_r/\text{\AA} < 0.20$  and  $W_r/\text{\AA} \geq 0.20$ ). The normalized spectrum (step black lines with  $1\sigma$  error bars) is reproduced by Voigt profiles sampling the posterior distribution of the parameters obtained by MC-ALF (solid red lines). Each individual CIV component is marked by a vertical red tick and shown as cyan dotted line.

then estimates the minimum number of Voigt components required to reproduce the observed flux. Each component is defined by the redshift, the Doppler parameter and the column density. We set priors restricting the line parameters between  $1 \leq b/(\text{km s}^{-1}) \leq 30$  for the Doppler parameter and  $12 \leq \log(N/\text{cm}^{-2}) \leq 16$  for the column density. To account for possible uncertainties in continuum-fitting, we multiply the normalized continuum by a constant (allowed to vary in the range  $0.98 - 1.02$ ) which is included as a free parameter. To improve the quality of the fit, we allow the spectral resolution to vary slightly around the nominal value. Specifically, the range extends over  $\pm 1 \text{ km s}^{-1}$  and  $\pm 5 \text{ km s}^{-1}$  for high-resolution (HIRES, UVES, MIKE) and moderate-resolution (X-SHOOTER, ESI) spectra, respectively. The model is then convolved with a Gaussian kernel to match the line spread function of the observed data. To reproduce the shape of blended absorbers, we introduce filler Voigt components that account for absorption lines physically uncorrelated with CIV doublets.

Once the Voigt model is computed for all the candidate doublets, we identify the significant detections by computing the rest-frame equivalent width for all the posterior samples returned by the chains of each MC-ALF fit. Filler components are excluded. Based on this estimate, we inspect again all the candidate doublets and consider significant detections those systems with an equivalent width of the weakest line,  $W_r^{1550}$  that, once compared to its error, is above  $3\sigma$ . This step leaves us with 264 systems at  $z > 3$ . All the selected doublets are visually inspected one last time to manually exclude heavy blended lines for which we cannot reliably reconstruct a unique model. We also exclude the weakest features that passed the automatic selection but appear to be arising from imperfect continuum normalization and for which the doublet line ratio deviates from the modelled one set by the ratio of the oscillator strengths. The final sample includes 220 CIV absorption-line systems with redshift  $3.0 \leq z \leq 4.3$  (median  $z \approx 3.31$ ; see Figure 3). In assembling this sample, all the components found within a velocity separation of  $\pm 500 \text{ km s}^{-1}$  from the highest column density one are considered as an individual absorption system. We show a summary of the final sample in Figure 2, where the doublets are plotted in the CIV redshift path of each sightline and sized as a function of the rest frame equivalent width. For each CIV system in the catalogue we provide a measure of the rest-frame equivalent width (median  $W_r^{1548} \approx 0.089 \text{\AA}$ ) and a measure of the kinematics traced by the line width in velocity space, defined by the interval enclosing the 90% of the optical depth (median  $\Delta v_{90} \approx 74.1 \text{ km s}^{-1}$ ). The CIV absorption systems included in this sample and their properties (redshift,  $W_r$  and  $\Delta v_{90}$ ) are listed in Table 1 and available as online material (see ).

To assess the completeness of this sample we compare the final observed equivalent width distribution from this search to known completeness-corrected functions from the literature. Specifically, we compute the equivalent width frequency distribution,  $f(W_r, X)$ , which counts the number of CIV systems per unit equivalent width per unit survey co-moving path,  $X$ . The uncertainties on the estimate of  $f(W_r, X)$  are derived as the 10<sup>th</sup> and 90<sup>th</sup> percentiles of the distribution obtained by bootstrapping over the sightlines with  $10^3$  repetitions. To gauge the completeness of our search, in Figure 4 we compare the observed equivalent width frequency distribution obtained for the CIV line at  $1548\text{\AA}$  in MAGG, as a function of the rest-frame equivalent width, with the completeness corrected function derived by Hasan et al. (2020) and Cooksey et al. (2013), which are selected as significant examples in the literature in terms of statistical modelling of  $f(W_r, X)$ . In detail, Hasan et al. (2020) inspected 369 quasar sightlines at  $1.1 \leq z_{\text{qso}} \leq 5.3$  observed with Keck/HIRES and VLT/UVES, compiling a sample of 1318 absorbers in the redshift range  $1.0 \leq z \leq 4.75$  that is 50% complete at  $W_r \geq 0.05 \text{\AA}$ . Cooksey et al. (2013) searched  $\approx 26000$  sightlines from the SDSS DR7 quasar catalogue at  $z_{\text{qso}} \geq 1.7$ . The resulting sample is a collection of 16459 absorbers with  $1.46 \leq z \leq 4.55$  that is 50% complete at  $W_r \geq 0.6 \text{\AA}$ .

According to the comparison shown in Figure 4, our  $f(W_r, X)$  is in good agreement with the observations reported in the literature. Overall, this good agreement validates the procedures adopted to extract our CIV sample. We also note that the slope of MAGG data starts decreasing around  $W_r \approx 0.08 \text{\AA}$  and flattens significantly at lower column densities, a feature we attribute to the progressively-increasing incompleteness of our sample. Moreover, the MAGG quasar spectroscopy and the data from Hasan et al. (2020) are comparable in quality, both being derived from echelle data at  $S/N \gtrsim 10$ . Therefore, if we take as reference the sensitivity function shown in figure 4 from Hasan et al. (2020) where the 50% completeness limits are highlighted for different redshift ranges, we can assume that the MAGG

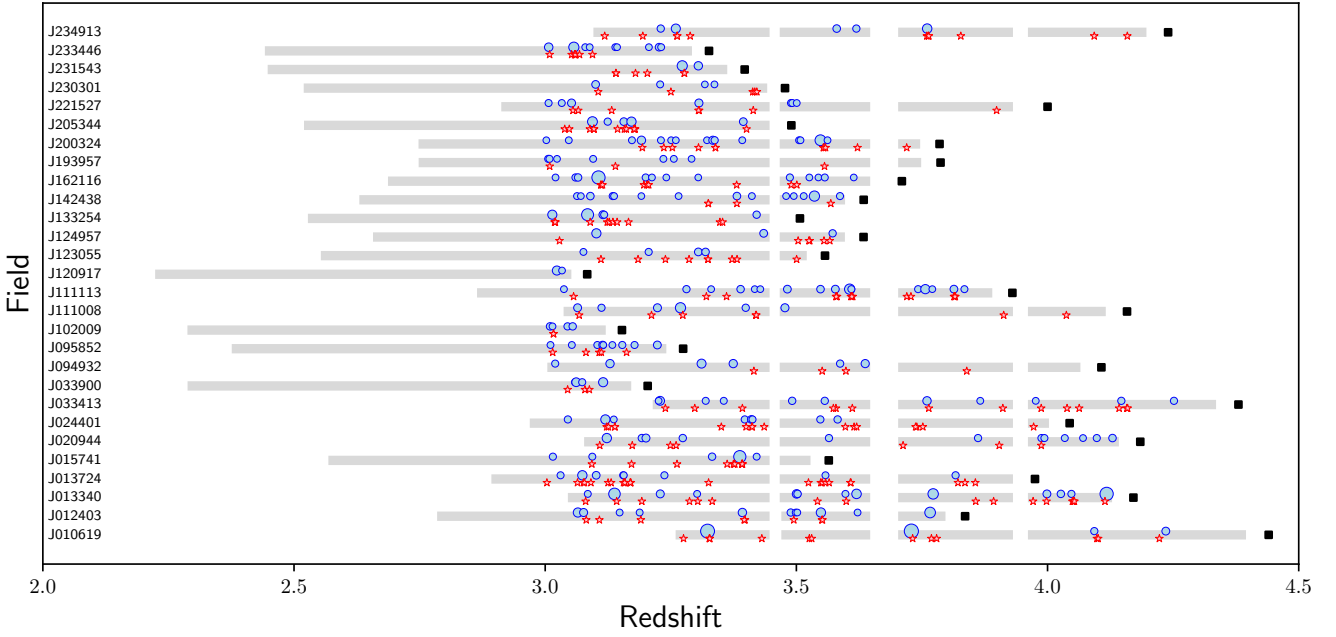


**Figure 2.** Summary of the final MAGG-C IV sample. The grey bands mark the searchable C IV redshift path of each sightline. The gaps correspond to known telluric bands we masked to avoid false positives. The doublets at  $z \geq 3$  are drawn as blue dots and sized proportionally to the equivalent width of each line. LAEs detected in the MUSE cubes  $z \geq 3$  and lying in the C IV redshift path are shown as red stars. The central quasar of each field is shown as a black square. A velocity window  $|\Delta v| < 3000 \text{ km s}^{-1}$  from the redshift of each quasar is also masked to avoid proximity effects.

Sightline	Instrument	$z$	$W_{1548} (\text{\AA})$	$\Delta v_{90} (\text{km s}^{-1})$
J010619+004823	MIKE	3.3232	$1.108 \pm 0.008$	$247.707 \pm 4.198$
J010619+004823	MIKE	3.7289	$1.146 \pm 0.013$	$285.509 \pm 14.692$
J010619+004823	MIKE	4.0931	$0.093 \pm 0.007$	$37.800 \pm 8.400$
J010619+004823	ESI	4.2354	$0.188 \pm 0.006$	$229.808 \pm 10.793$
J012403+004432	UVES	3.0650	$0.393 \pm 0.003$	$155.025 \pm 2.501$

**Table 1.** List of the properties ( $z$ ,  $W_{1548}$ ,  $\Delta v_{90}$ ) measured for the C IV absorption line systems detected at  $3\sigma$  and included in the sample studied in this work. We also provide information about the sightline and the spectrum in which each absorber is detected. Only the first five lines are shown here, the full table is available as online supplement.

C IV is approximately 50% complete around an equivalent width of  $W_r^{1548} \approx 0.05 \text{ \AA}$ , and generally complete for  $W_r^{1548} \gtrsim 0.08 \text{ \AA}$ .

### 3.2 Catalogue of Si IV absorption lines

With the goal of identifying an additional tracer of ionized gas comparable to C IV in the wavelength range covered by our observations, the same strategy developed to assemble the catalogue of C IV doublets is implemented to search and analyze Si IV  $\lambda\lambda$  1393, 1402 absorption-line systems. A first sample of 145 Si IV absorbers with redshift  $2.9 \lesssim z \lesssim 4.4$  is built by visually inspecting the quasar spectra. Running MC-ALF code with the same priors and setting defined for C IV doublets, we fit each of these lines and estimate the minimum number of Voigt components required to reproduce the observed flux. We exclude all the candidates that do not show a characteristic rest wavelength separation of  $\approx 9 \text{ \AA}$  and optical depth ratio  $\tau_{1393}(\nu)/\tau_{1402}(\nu) \approx 2$  (as set by the ratio of the oscillator strengths) between the two transitions of the doublet in the unsaturated regime. The final sample includes 108 Si IV systems with a rest-frame equivalent width of the weakest part of the doublet,  $W_r^{1402}$ , detected above  $3\sigma$ .

For each absorber we provide a measure of the redshift (median  $z \approx 3.45$ ), rest-frame equivalent width (median  $W_r^{1393} \approx 0.077 \text{ \AA}$ ) and the width in velocity space (median  $\Delta v_{90} \approx 64.7 \text{ km s}^{-1}$ ). The properties of these systems are listed in Table 2 and available as online material, while a summary of the distribution of these properties is shown in Figure 3, with median values listed in Table 3. To estimate the completeness of the sample, we derive the equivalent width frequency distribution,  $f(W_r, X)$ , which we compare with the C IV one in Figure 4. We note that the shape of the Si IV is similar to what we obtained for the C IV sample, and we conclude that the completeness estimates above can be also applied to the Si IV catalogue, which we take to be  $\approx 50\%$  complete for  $W_r^{1393} \gtrsim 0.05 \text{ \AA}$ , and complete for  $W_r^{1393} \gtrsim 0.08 \text{ \AA}$ .

### 3.3 Identifying galaxies in MUSE data

To link the ionized gas detected in absorption via C IV with the surrounding galaxy population, we proceed to compile catalogues of galaxies detected in the MUSE data. The first step is to identify continuum-bright galaxies. Lofthouse et al. (2020) and MAGG IV provide extensive details on how continuum sources are handled.

Sightline	Instrument	$z$	$W_{1548}$ (Å)	$\Delta v_{90}$ (km s <sup>-1</sup> )
J010619+004823	MIKE	4.2348	$0.065 \pm 0.009$	$55.649 \pm 10.501$
J012403+004432	UVES	3.3922	$0.106 \pm 0.002$	$79.997 \pm 2.500$
J012403+004432	UVES	3.5488	$0.321 \pm 0.002$	$197.532 \pm 2.501$
J012403+004432	UVES	3.6755	$0.388 \pm 0.002$	$115.727 \pm 1.874$
J012403+004432	UVES	3.7661	$0.057 \pm 0.001$	$105.014 \pm 1.250$

**Table 2.** Same as Table 1 for the Si iv absorbers detected at  $3\sigma$ . The first 5 lines are shown, while the full table is available as online material.

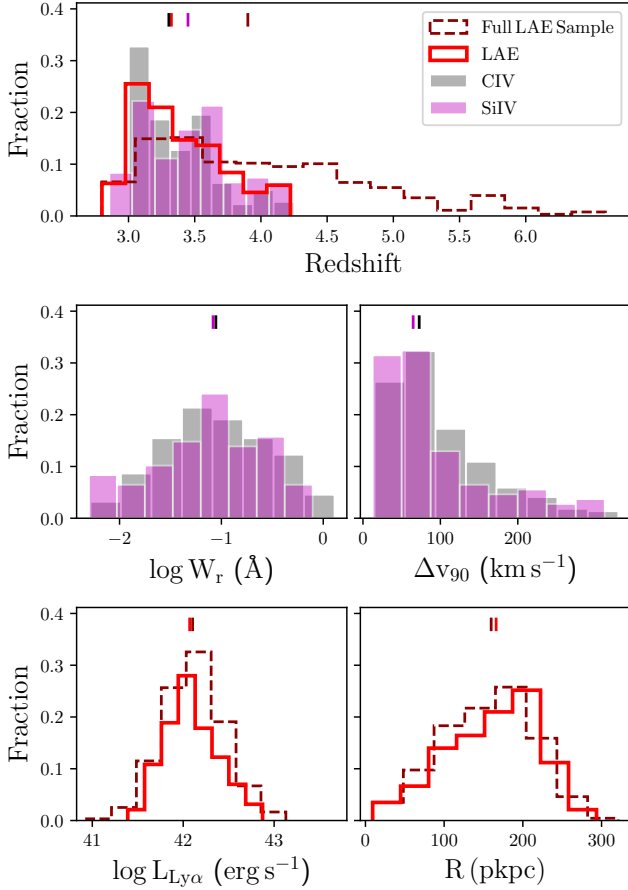


**Figure 3.** Summary of the properties measured for the C iv (black) and Si iv (magenta) doublets (redshift, rest-frame equivalent width and velocity width) and those of the emitters (redshift,  $L_{\text{Ly}\alpha}$  luminosity and impact parameter) identified in the MAGG fields at  $SNR > 7$  (dashed red line) and in the absorbers redshift path (solid red line). Vertical ticks mark the median of each distribution.

Property	$z$	$W_r$ (Å)	$\Delta v_{90}$ (km s <sup>-1</sup> )
C iv	3.31	0.089	74.1
Si iv	3.45	0.077	64.7

**Table 3.** Summary of the median properties of C iv and Si iv absorbers, where  $W_r$  refers to the strongest part of each doublet.

Briefly, we first run *SEXTRACTOR* (Bertin & Arnouts 1996) on the reconstructed white-light image obtained by collapsing the cube along the wavelength axis. We then extract 1D spectra from the cubes following the 2D segmentation maps generated by *SEXTRACTOR* and

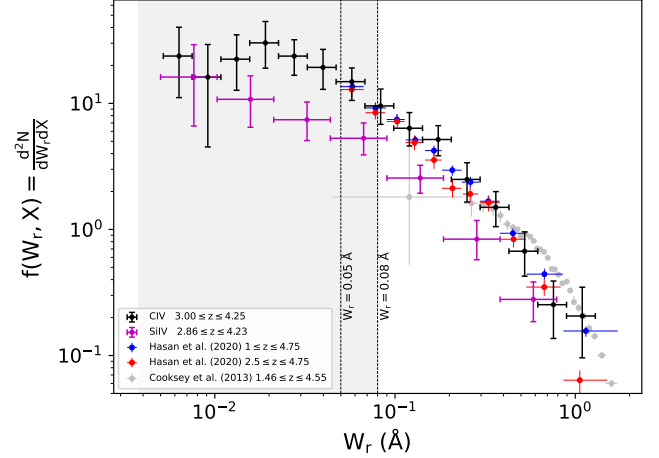


**Figure 4.** Equivalent width frequency distribution function  $f(W_r, X)$  for the MAGG C iv sample (black dots). Vertical error bars are the 10<sup>th</sup> and 90<sup>th</sup> percentiles from bootstrap re-sampling, while horizontal error bars reproduce the width of each redshift bin. The MAGG sample is compared with the completeness-corrected results from Hasan et al. (2020) (red and blue dots) and Cooksey et al. (2013) (grey dots). The shaded region mark the equivalent width interval over which our search suffers from incompleteness. Also shown (magenta dots), the equivalent width distribution for the Si iv line at 1393Å.

use the M. Fossati branch<sup>1</sup> of the *MARZ* tool (Hinton et al. 2016) to measure spectroscopic redshifts for the extracted sources. At the end of this procedure, we identify over 1200 sources with redshift, corresponding to 90% completeness down to  $\approx 24.85$  mag.

With the purpose of extending the study of the CGM at high redshift to lower-mass star-forming galaxies, we next search the MUSE field of view for LAEs, here defined as any galaxy emitting bright  $\text{Ly}\alpha$  emission lines on a typically faint or non-detected continuum. Following the procedure described by Lofthouse et al. (2020) and MAGG IV, we first run the three-dimensional automatic extraction performed by *CUBEx* to identify connected groups of voxels (three-dimensional pixels) that lie above a defined  $S/N = 3$  on the cubes with subtracted continuum sources, including both galaxies and the quasar point spread function (PSF). For the subtraction of the PSF, we follow the non-parametric method detailed in section 3.1 of Arrigoni Battaia et al. (2019).

The presence of residuals from the continuum of stars and galaxies is mitigated by masking the spatial position of all the continuum-detected sources with known redshift (see Borisova et al. 2016). This process produces a set of cubes free of any continuum contamination which can be used to build a sample of compact LAEs.

More specifically, to be identified by the *CUBEx* algorithm, each line emitter candidate requires: i) a minimum volume, imposed by a

<sup>1</sup> matteofox.github.io/Marz

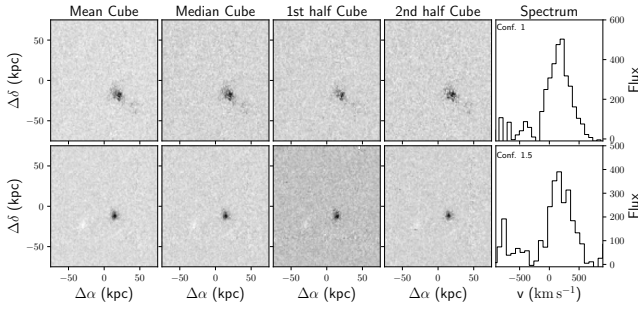


**Figure 5.** Examples of high-confidence LAEs identified in the fields. Columns from left to right show the images extracted by CUBEX in the mean, median and the half-exposure cubes. The last column shows the 1D spectra limited to the wavelength channels centered on the redshift of the Ly $\alpha$ . The flux is measured in units of  $10^{-20}$  erg s $^{-1}$  cm $^{-2}$  Å $^{-1}$ .

number of voxels  $\geq 27$  above the threshold  $S/N$ ; ii) a lower limit of the width in the wavelength direction of at least 3 wavelength channels; iii) an upper limit in the wavelength direction of 20 channels to exclude any possible contamination from residuals arising in continuum sources. Since these selection criteria do not remove all the contaminants, such as residual cosmic rays, visual inspection of each extracted LAE is required to weed out the remaining contaminants. Compact LAEs are also distinguished from residuals of sky lines, significant noise fluctuations at the edge of the field or lower redshift emission lines (typically, C iv  $\lambda\lambda$  1548, 1550; C III]  $\lambda\lambda$  1907, 1909; [O II]  $\lambda\lambda$  3727, 3729; [O III]  $\lambda$  5008; H  $\beta$   $\lambda$  4862). In order to assure the best quality sample, a first classification is performed by two authors (MG and EL) and confirmed by other two authors (MF and MFo), independently.

The visual inspection of the 28 MAGG fields results in a sample of 994 LAEs at redshift  $2.81 \leq z \leq 6.60$  and detected at integrated  $S/N \geq 7$ . All the identified emitters are divided into three confidence levels, which updates the original classification by Lofthouse et al. 2020 based on the integrated signal-to-noise ratio (ISN) and confidence of the classification: i) *Confidence 1* class contains emitters with  $ISN \geq 7$  which are confidently detected and unambiguously recognized as LAE due to e.g. asymmetric line profiles, or presence of additional absorption lines other than Ly $\alpha$ ; the *confidence 1.5* sub-class contains instead confidently-detected sources at  $ISN \geq 7$  that are recognized as LAEs but for which there is less confidence in ruling out lower-redshift sources (e.g. with double peaked profiles possibly mimicking [OII] emitters but not recognized as such due to the lack of other oxygen lines or with atypical line separations/ratios); ii) *Confidence 2* emitters have  $ISN < 7$  but are deemed to be LAEs, with a sub-class, marked as *confidence 2.5*, containing any system that is noisy and shows anomalies due to noise in its segmentation map and half-exposure cubes; iii) *Confidence 3* emitters are recognized as LAEs but lie at the edge of the FoV in noisy regions or only partially overlap with the detector, making any measurement of their properties (e.g. integrated flux, centroid) unreliable. Figure 5 provides an example of sources classified under class 1 and 1.5, which are used in this work. Based on this classification, we assemble a sample of LAEs detected at higher integrated  $S/N$  ( $ISN \geq 7$ ) compared to the MAGG IV sample ( $ISN \geq 5$ ) by excluding all the emitters with confidence  $\geq 2$  from the following analysis. The final sample includes 921 high-confidence LAEs.

For each LAE included in the final MAGG sample, we derive a measure of the redshift, Ly $\alpha$  luminosity and projected distance from

the line-of-sight (i.e., the impact parameter). For this purpose, from the 3D segmentation cubes produced by CUBEX, the 1D spectra is extracted along the full wavelength range and used to derive an estimate of the redshifts. Ly $\alpha$  photons are known to be subject to radiative transfer effects which affect both their spatial and frequency distribution, resulting in typical asymmetric or double-peaked emission lines. Therefore, we apply the following convention (see also Verhamme et al. 2018; Muzahid et al. 2020, MAGG IV): in case of a double-peaked line, we take the redshift of the red peak; if a single peak is observed instead, we assume that this is the red peak since the blue one is more easily absorbed.

To derive the Ly $\alpha$  luminosity we adopt instead a curve of growth (CoG) analysis. This method better adapts to the typical Ly $\alpha$  emission profile that is spatially extended and characterized by two distinct components: a bright core and a faint diffuse halo (Wisotzki et al. 2016; Leclercq et al. 2017). The latter is easily excluded in the flux measured from the segmentation cube at moderate  $S/N$ . Here, we follow the method described by Fossati et al. (2019) (see also Marino et al. 2018). For each emitter we build a pseudo narrow-band image by summing up the spectral channels within  $\pm 14$  Å from the source redshift and masking the neighbours. A series of circular apertures with increasing radii, over which we produce the CoG flux, is centered on the CUBEX coordinates of each source. As a result, we take as reliable CoG flux the estimate obtained at the last radius where the total flux increases by more than 2.5% than the previous step. All the diagnostic plots are visually inspected to check that no contamination other than the LAEs has been included in the fluxes. Fluxes are then corrected for Milky Way extinction using the re-calibrated extinction map (Schlafly & Finkbeiner 2011) and assuming the Milky Way extinction law by Fitzpatrick (1999). Finally, we compute the luminosity distance at the redshift of each source and convert the total flux into a Ly $\alpha$  luminosity. A complete list of the Ly $\alpha$  emitters identified in the MAGG survey at  $SNR > 7$ , including a measure of the redshift, Ly $\alpha$  luminosity and impact parameter, is provided in Table 4 and available as online material.

In the whole MAGG sample, we identify 292 LAEs lying in the C iv redshift path. This subset also includes Ly $\alpha$  emission from 23 galaxies detected in continuum and forms the candidates for associations with the absorbers. Although we provide a complete survey of UV-selected galaxies, including continuum-detected LBGs and LAEs, our sample significantly favors line emitters. Thus, additional  $z > 3$  sources, e.g. LBGs with absorption features but not Ly $\alpha$  emission (1 detected in C iv redshift path), passive or heavily obscured galaxies, are not well represented in this work. In Figure 3 and Table 5 we summarize the properties measured for LAEs (redshift and Ly $\alpha$  luminosity) in the full MAGG sample and in the sub-set lying in the C iv redshift path. The latter are observed in a redshift range  $2.80 \leq z \leq 4.23$ , have a median  $z \approx 3.24$  ( $z \approx 3.91$  for the full MAGG sample) and emit a luminosity  $41.39 \lesssim \log(L_{Ly\alpha}/\text{erg s}^{-1}) \lesssim 42.87$ , with a median  $\log(L_{Ly\alpha}/\text{erg s}^{-1}) \approx 42.07$  (median  $\log(L_{Ly\alpha}/\text{erg s}^{-1}) \approx 42.10$  for the full MAGG sample). The emitters are detected at a projected distance from the line-of sight  $20 \lesssim R/\text{kpc} \lesssim 295$ , with a median  $R \approx 166$  kpc ( $R \approx 160$  kpc for the full MAGG sample).

### 3.4 Identifying galaxy groups

According to the hierarchical scenario of structure formation, galaxies assemble in groups or clusters, with only a fraction evolving in isolated environments. In dense galaxy environments, interactions between galaxies and with the surrounding medium are observed

Field	RA (deg)	DEC (deg)	$z$	$\log[L_{\text{Ly}\alpha}/(\text{erg s}^{-1})]$	$R$ (pkpc)	SNR	Confidence
J010619+004823	16.5788	0.8118	2.9263	$41.620 \pm 0.083$	157	8.3	1.0
J010619+004823	16.5834	0.8042	3.1082	$42.289 \pm 0.023$	112	20.4	1.0
J010619+004823	16.5860	0.8001	3.1213	$41.627 \pm 0.099$	242	8.5	1.0
J010619+004823	16.5834	0.8075	3.2081	$42.033 \pm 0.036$	95	13.9	1.0
J010619+004823	16.5782	0.8011	3.2112	$42.169 \pm 0.044$	159	15.0	1.0

**Table 4.** List of the LAEs detected in MAGG at  $\text{SNR} \geq 7$ . Information of the sightline, coordinates, SNR and confidence from our classification are included as well as the properties we measured (redshift  $z$ , luminosity  $\log[L_{\text{Ly}\alpha}/(\text{erg s}^{-1})]$ , projected distance to the quasar  $R$ ). Typical errors for redshifts are of the order of  $(6 - 7) \times 10^{-4}$ . Only the first five lines are shown here: the full table is provided as online material

Property	$z$	$\log[L_{\text{Ly}\alpha}/(\text{erg s}^{-1})]$	$R$ (kpc)
Full Sample	3.91	42.10	160
In C IV z-path	3.24	42.07	166

**Table 5.** Summary of the median properties of LAEs reported for the full sample and for the emitters detected in the C IV redshift path.

to affect the properties of different gas phases of the CGM, both at low and high redshift (see e.g., [Nielsen et al. 2018](#); [Fossati et al. 2019](#); [Dutta et al. 2020](#); [Muzahid et al. 2021](#)). Therefore, a better understanding of the gas-galaxy connection and co-evolution requires galaxy groups to be identified in the MAGG survey. For this purpose, without including any constraint on the halo mass, we recognize a galaxy to be part of a group if it is not isolated within a line-of-sight separation  $|\Delta v| \leq 500 \text{ km s}^{-1}$  in the MUSE FoV. By linking galaxies with this criterion, we identify 53 groups in the CIV absorbers redshift path shown in Figure 2 (152 in the full MAGG sample) so that  $\approx 47\%$  of the galaxies are part of a group ( $\approx 41\%$  for the full MAGG sample). The majority of these identified groups ( $\approx 57\%$ ) are composed of two galaxies ( $\approx 61\%$  for the full MAGG sample), but groups of three to six members (seven for the full MAGG sample) are also found.

## 4 RESULTS

### 4.1 Measuring correlations between C IV absorbers and LAEs

#### 4.1.1 Connecting C IV absorbers with galaxies

To establish the extent with which the detected C IV trace ionized gas in proximity of LAEs, we cross-match the catalogue of C IV absorbers with the one of the LAEs in redshift space. For this purpose, we center on each absorption system and we search for the galaxies within  $\pm 1000 \text{ km s}^{-1}$  along the line of sight, reserving the definition of a more stringent criterion (i.e., a smaller velocity separation) for the following analysis. In Figure 6 we show the gas-galaxy connections as a function of the line-of-sight separation (horizontal axis) and as a function of the transverse distance (vertical axis). We distinguish between the LAEs detected with high confidence (red dots) and those observed at the edge at the field of view (blue dots). We also highlight the galaxies associated to C IV absorbers that are connected to Lyman limit systems (LLSs) from the MAGG IV paper (gold dots). This sample includes 127 LAEs associated to 61 absorption-line systems detected at  $S/N \geq 5$ , 79 detected at  $S/N \geq 7$ . As  $\approx 70\%$  of these LAEs are in the vicinity of a C IV absorber, this fraction is also independently recovered by our search.

In order to characterize the significance of the gas-galaxy connection, we build a control sample (in grey within Figure 6) which aims at reproducing the typical distribution of the galaxies around random regions in the Universe not selected in absorption, where we do not necessarily expect C IV systems. To do so, we bootstrap

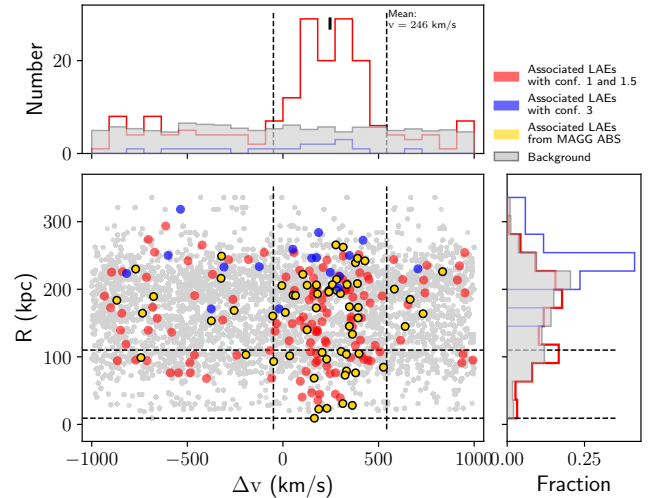


**Figure 6.** Distributions of LAEs near C IV absorbers as a function of line-of-sight velocity separation and projected distance. The high-confidence LAEs are marked in red, while the galaxies at the edge of the field are in blue. In gold, we mark the galaxies connected to C IV absorbers that are also associated to high-column hydrogen absorbers from the MAGG IV paper. A random population of LAEs, which is representative of background and foreground population at larger velocity separations from C IV absorbers, is shown for reference in grey. The dashed lines highlight the regions where a clear excess signal of LAEs around C IV is detected over the uncorrelated background.

over the sightlines, randomly selecting 28 fields from the full MAGG sample for a total of  $10^3$  realizations. At each iteration and in each selected field, we measure the distance of LAEs to the redshift of a real C IV absorber, which is however randomly extracted from all the systems detected in the remaining sightlines. Using this technique, we are effectively building a control sample using real data (both for LAEs and C IV absorbers), optimally controlling for systematics like the presence of sky line residuals.

Examining the distribution of velocities along the line of sight in the upper histogram of Figure 6, we observe a clear excess of LAEs near C IV absorbers compared to the random sample distribution at offset velocities of  $\Delta v = 0 - 500 \text{ km s}^{-1}$ . Assuming that the galaxies are randomly distributed relative to the line of sight, one would expect to find a relative velocity separation between LAEs and C IV that is symmetric around the C IV redshift. However, being based on the Ly $\alpha$  emission line, our estimate of the galaxies redshift suffers from the resonant scattering that affects the frequency and spatial distribution of the Ly $\alpha$  photons emitted by the galaxies. To measure this offset, we fit the velocity separation distribution with a Gaussian model plus a background as a function of the velocity separation, obtaining



a mean value of  $\Delta v_{\text{Ly}\alpha} \approx 246 \text{ km s}^{-1}$ . Similar trends are indeed observed in the literature. [Rakic et al. \(2011\)](#) measured an offset  $\Delta v_{\text{Ly}\alpha} \approx (295 \pm 30) \text{ km s}^{-1}$  between  $z \sim 2.3$  LBGs and stacked H I absorption lines. More recently, [Muzahid et al. \(2020, 2021\)](#) derived a velocity offset of the order of  $\Delta v_{\text{Ly}\alpha} \approx (171 \pm 8) \text{ km s}^{-1}$  between LAEs and stacked H I absorption at redshift  $z \approx 3$ . They also obtained a similar velocity offset, although with larger uncertainties, between LAEs and stacked C iv profile. Lastly, the velocity separation between LAEs and H I absorbers observed in MAGG IV peaks at  $\Delta v_{\text{Ly}\alpha} \approx 250 \text{ km s}^{-1}$ . In light of this result, in the following we establish associations by correcting the redshift of the LAEs for the mean offset  $z'_{\text{LAE}} = z_{\text{Ly}\alpha} - \Delta v_{\text{Ly}\alpha} (1 + z_{\text{Ly}\alpha})^{-1} c^{-1}$ .

Since the majority of the LAEs is observed within  $0 - 500 \text{ km s}^{-1}$  from the absorber, we can restrict the velocity window in which a galaxy is considered associated with an absorber to build a sample of connected systems. In the following, we thus perform our analysis on galaxies that are  $\pm 500 \text{ km s}^{-1}$  from a C iv absorber, an interval that becomes  $-254 < \Delta v / (\text{km s}^{-1}) < 746$  once corrected for the Ly $\alpha$  velocity offset. We detect at least one LAE within this velocity separation for 79 C iv absorbers, corresponding to a detection rate of  $36 \pm 5$  per cent (79/220).

The right histogram of Figure 6 shows instead the transverse separation distribution between the C iv absorbers and the LAEs. The overall trend is consistent with an increasing number of detections with increasing area of the annulus ( $\propto R^2$ ), and a steep decrease due to edge effects at  $R > 200 \text{ kpc}$ . Although with a significant scatter, only a very small excess of LAEs is detected at transverse separations  $R < 100 \text{ kpc}$  over the control distribution, suggesting that some, but not many, C iv systems preferentially arise from the inner CGM of the associated galaxy. Overall, however, the impact parameter distribution looks similar to the one of the control population.

In summary, the connection in redshift space between the C iv absorbers and the LAEs reveals that a factor of  $\approx 2.6$  more galaxies are observed within  $\pm 500 \text{ km s}^{-1}$  from an absorption line system relative to the number of galaxies detected in random regions of the Universe. This result implies that the C iv absorbers do not trace a random region of the Universe, but regions with a preference for hosting LAEs.

#### 4.1.2 Number density of LAEs associated to C iv absorbers

The detection of a local clustering signal along the line-of-sight is indicative of the existence of a physical connection between the C iv absorbers and the LAE population. In this section, we measure statistically the LAE number density by deriving the luminosity function (LF),  $\phi(L)dL$ . A comparison of LFs from different environments (e.g., in the field or near C iv absorbers) further allows us to study the extent to which the LAE number density depends on the proximity to the absorption-line systems. The procedure we follow in the computation of the LF is described in detail by [Fossati et al. \(2021\)](#). We assume any redshift dependence to be negligible in the probed range  $3.0 < z < 4.5$  as, based on the results from [Herenz et al. \(2019\)](#), no significant redshift evolution is observed in the wide range  $2.9 < z < 6.0$ . In the analysis, we compare a non-parametric estimator of the LF,  $1/V_{\text{max}}$  from [Schmidt \(1968\)](#) and [Felten \(1976\)](#), with the results obtained from fitting the full sample with no binning using a parametric Schechter function.

The  $V_{\text{max}}$  non-parametric estimator relies on the survey selection function  $f_c(L, z)$ , defined as the probability to find an LAE with a given luminosity at a given redshift. The selection function is derived performing a simulation based on the injection of 500 mock

LAEs and measuring the fraction of sources we recover running CUBEx and applying our search algorithm. The flux, redshift and spatial positions of the mock sources are tabulated. This procedure is repeated for 1000 iterations over all the MAGG fields, with the only exception of J142438+225600 that is lensed ([Patnaik et al. 1992](#)).

In order to compute the effective co-moving area of the survey, we re-scale the MUSE field area by a factor  $\delta_{\text{obs}}(z)$  that accounts for the number of fields where we searched for LAEs at a given redshift. Therefore, we center on the redshift of each C iv absorber and consider only the contributions from the redshift range enclosed within  $\pm 500 \text{ km s}^{-1}$  from the absorber. The factor  $\delta_{\text{obs}}(z)$  is equal to zero in the ranges excluded from the searched path. The luminosity bins are 0.2 dex wide. We limit the uncertainties on the weight given by  $V_{\text{max}}$  by excluding from the analysis all the LAEs identified below  $f_c(L, z) < 0.1$ . The results of the luminosity function using this non-parametric estimate for the LAEs connected to the C iv absorbers are shown as black dots in Figure 7 with respective uncertainties.

We also derive a parametric estimate of the LAE luminosity function by fitting a Schechter function ([Schechter 1976](#)) to the non-binned sample:

$$\phi(L) = \ln(10) \phi^* 10^{(\log L - \log L^*)(1+\alpha)} \exp[-10^{(\log L - \log L^*)}]. \quad (1)$$

For the fit, we proceed as described in [Fossati et al. \(2021\)](#). The result from the parametric modelling of the luminosity function is shown as a solid black line in Figure 7 for the LAEs associated to the C iv absorbers, with the shaded areas marking the  $1\sigma$  confidence intervals. In order to study how being in the vicinity of the C iv absorbers affects the LAEs number density, we apply the procedure described above to a sample of LAEs from a random sample (referred to as ‘‘MAGG field’’) that is not selected by its proximity to a specific tracer. This field sample is built by including 617 LAEs detected in the range  $3.0 < z < 4.5$ , corresponding to the redshift interval in which we observe C iv absorption in MAGG. The non-parametric estimate and the parametric Schechter fit are shown in red in Figure 7.

To test the consistency of the field luminosity function with previous determinations, the results are compared to the literature. The estimate from [Herenz et al. \(2019\)](#) is based on a sample of 237 LAEs spread in a redshift range  $2.9 < z < 6.0$  and detected in  $\sim 1$  hour of MUSE observations. Here we report their results for a sub-sample restricted to the range  $3.0 < z < 4.0$ , chosen to be consistent with the C iv absorbers detected in MAGG. To extend the comparison at lower luminosities, we consider the results from [de La Vieuville et al. \(2019\)](#). This sample contains 156 LAEs at  $2.9 < z < 6.7$  with luminosities  $39 \lesssim \log(L_{\text{Ly}\alpha}/\text{erg s}^{-1}) \lesssim 43$ . As done before, we consider the luminosity function derived for a sub-sample of LAEs detected in the range  $2.9 < z < 4.0$ . As we adopt  $H_0 = 67.7 \text{ km s}^{-1} \text{ Mpc}^{-1}$  while the literature studies chose  $H_0 = 70 \text{ km s}^{-1} \text{ Mpc}^{-1}$ , the luminosity functions derived from these two samples are scaled to be consistent with our cosmological parameters (a  $\lesssim 10\%$  correction). As shown in Figure 7, the luminosity function derived for the MAGG field sample is consistent within the uncertainties with the results from the literature. Furthermore, the large size of the MAGG field sample provides a statistically significant modelling of the luminosity function at  $3.0 < z < 4.5$  for a population of lower-mass star forming galaxies traced by LAEs with halo mass  $M_H \approx 10^{11} M_\odot$  compared to, e.g., continuum detected populations like LBGs with  $M_H \approx 10^{12} M_\odot$  (see Section 5.1.2 for additional details).

Having computed the field luminosity function, we derive an estimate of the LAE number density in the vicinity of the C iv ab-

Sample	S/N limit	$\log[L^*/(\text{erg s}^{-1})]$	$\alpha$	$\log[\phi^*/(\text{Mpc}^{-3} \text{dex}^{-1})]$	$\log(I/\text{Mpc}^{-3})$
QSO	5	$42.573 \pm 0.221$	$-1.164 \pm 0.319$	$-1.429 \pm 0.276$	-1.239
ABS	5	$42.558 \pm 0.242$	$-1.350 \pm 0.309$	$-1.788 \pm 0.343$	-1.540
C iv	7	$42.575 \pm 0.212$	$-1.418 \pm 0.323$	$-2.175 \pm 0.163$	-1.887
Field	7	$42.471 \pm 0.082$	$-1.345 \pm 0.158$	$-2.243 \pm 0.123$	-2.262

**Table 6.** Parameters of the Schechter function describing the LAE luminosity function around the different tracers studied in MAGG. The last column is the integral of the Schechter function computed at luminosities  $\log[L_{\text{Ly}\alpha}/(\text{erg s}^{-1})] \geq 41.8$ .

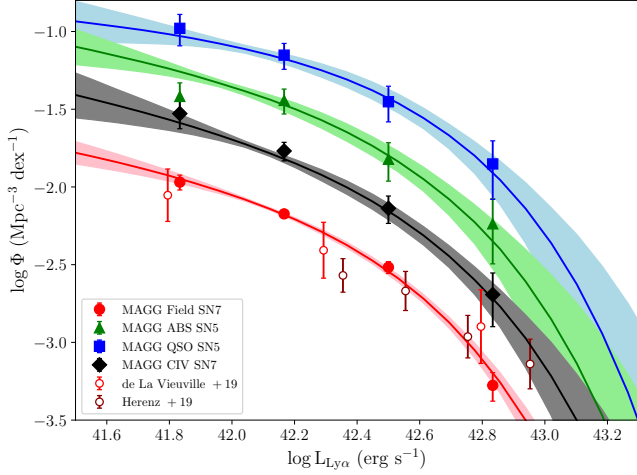


**Figure 7.** Luminosity function derived for the LAEs associated to the C iv absorbers (black diamonds) in a luminosity range  $41.5 < \log(L_{\text{Ly}\alpha}/\text{erg s}^{-1}) < 43.0$ , using non-parametric (data points) and parametric (lines) estimates. The results from this work are compared with the results from a field control sample (red circles), the environment of high-column density H I systems (green triangles) from MAGG IV, and the environment around quasars from Fossati et al. (2021) (blue squares). For comparison, we also show the field luminosity function from Herenz et al. (2019) and de La Vieuville et al. (2019).

sorbers extending the comparison with other populations in MAGG. In MAGG IV, we studied the luminosity function of 97 LAEs detected within  $\pm 500 \text{ km s}^{-1}$  from 45 strong hydrogen absorbers selected as tracers of the dense CGM (the “MAGG ABS” sample). We note the MAGG ABS and the MAGG C iv samples are partially overlapping (not all C iv absorbers are associated to LLSs, see Section 5.2), thus the comparison is not independent. In addition, the “MAGG QSO” sample from Fossati et al. (2019) includes 86 LAEs found within  $\pm 500 \text{ km s}^{-1}$  from the central quasar of each field. For consistency, these two samples include LAEs detected in a redshift range  $3.0 \lesssim z \lesssim 4.0$  that is comparable to the MAGG C iv sample. The use of different  $S/N$  thresholds for the various samples ( $S/N \geq 5$  for MAGG ABS and QSO samples,  $S/N \geq 7$  for MAGG C iv and field samples) is justified by noticing that a higher  $S/N$  limit does not change the overall shape either of the non-parametric or the parametric estimate (as expected from the completeness correction based on the survey selection function), but only broadens the  $1\sigma$  confidence regions. The best Schechter parameters estimated from the parametric fit are listed in Table 6 for each MAGG sample.

The parameters  $\log L^*$  and  $\alpha$  of the different samples are all consistent within  $1\sigma$ . This suggests that the overall shape of the LAE luminosity function does not depend on which tracer is used to select the environment within which these galaxies reside. Despite the normalization constant,  $\phi^*$ , having the units of a LAEs number density, it is not computed at fixed luminosity and thus can-

not be directly compared among the different tracers. Therefore, we derive a measure of the relative LAEs overdensity by computing the integral  $I$  of the Schechter function over the luminosities  $\log[L_{\text{Ly}\alpha}/(\text{erg s}^{-1})] \geq 41.8$ . The results are shown in Table 6, where we find that the cumulative number of LAEs at close separation from the C iv absorbers is a factor  $\approx 2.4$  higher than the field. The MAGG ABS sample is associated to an intermediate LAE overdensity that is a factor  $\approx 2.2$  higher than the C iv sample. Finally, the normalization for the MAGG QSO sample is a factor  $\approx 4.5$  higher relative to the MAGG C iv sample and  $\approx 2.0$  compared to the MAGG ABS sample, pinpointing a richer overdensity of LAEs.

In conclusion, the analysis of the distribution of LAEs in velocity space and of the luminosity function in different environments underscores a systematic preference for LAEs to cluster around C iv absorbers with equivalent width  $\geq 0.05 \text{ \AA}$ , implying in turn that C iv systems do not always trace average regions of the Universe but, often, regions near LAEs. Indeed, as we will show in detail below,  $\approx 36\%$  of the total number of the absorbers is in fact associated to at least an LAE, with  $\approx 48\%$  of these C iv systems being associated to multiple LAEs.

## 4.2 Correlation functions

Having established the presence of an overdensity of LAEs near C iv absorbers, we now quantify the connection between the galaxies and the ionized gas statistically, by deriving the LAEs auto-correlation and the LAEs-absorber cross-correlation functions. The main goal of this analysis is to establish whether the C iv absorbers are physically connected to the galaxies, and actually populate halos, or whether they are preferentially observed in IGM filaments. To do so, following the interpretation of Adelberger et al. (2003, 2005), we exploit the Cauchy-Schwarz relation that compares the galaxy-galaxy and the absorber-absorber auto-correlation functions,  $\xi_{\text{GG}}(r)$  and  $\xi_{\text{AA}}(r)$  respectively, with the galaxy-absorber cross-correlation function,  $\xi_{\text{GA}}(r)$ :

$$\xi_{\text{GA}}^2 \leq \xi_{\text{GG}} \xi_{\text{AA}}. \quad (2)$$

This relation can be used to compare the galaxies and absorbers underlying matter density distribution since the equality holds if the C iv absorbers and the galaxies originate from density fluctuations that are linearly dependent. A similar approach has been widely adopted in the literature to measure the clustering of the LBGs at redshift  $z \sim 3$  (Adelberger et al. 2003, 2005; Bielby et al. 2011) and establish the correlation of galaxies with various ions, such as H I and O VI at redshift  $z < 1$  (Chen & Mulchaey 2009; Tejos et al. 2014; Finn et al. 2016; Prochaska et al. 2019) or C iv at  $z \sim 3$  (Adelberger et al. 2003, 2005). Furthermore, by relying on the  $k$ -estimator (Adelberger et al. 2005) that counts the number of pairs without requiring the assembly of a random sample as an alternative to the typical two-point correlation function, Diener et al. (2017) and Herrero Alonso et al. (2021) detected, for the LAEs auto-correlation, a clustering signal extended up to  $\approx 3.0 \text{ pMpc}$  in a large sample of emitters at  $3.0 \lesssim z \lesssim 6.0$ .

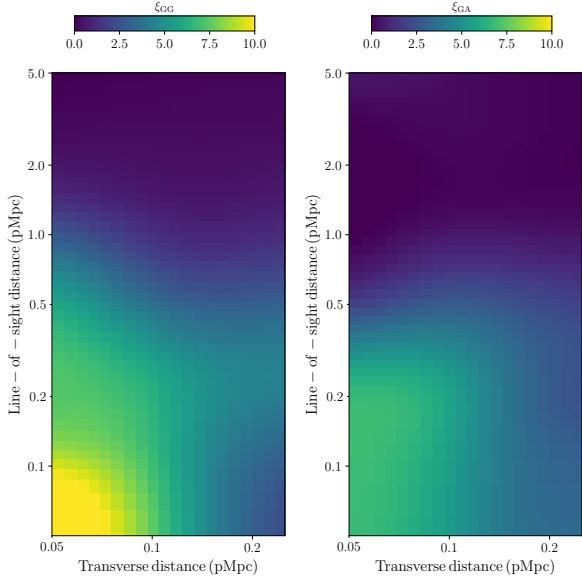


**Figure 8.** Two dimensional auto-correlation function for LAEs (left panel) and LAE-C iv cross-correlation function (right panel).

#### 4.2.1 Formalism and random samples

The correlation functions are derived as a function of the pairs projected distance  $R$  and their separation along the line-of-sight  $R_{\text{los}}$ . The latter is computed as velocity separation and converted into a distance assuming pure Hubble flow. We use the [Davis & Peebles \(1983\)](#) estimator to compute both the auto-correlation and the cross-correlation functions, which compares the number of data-data pairs and random-random pairs at a given  $R$  and  $R_{\text{los}}$ .

For the computation of the random-random pairs, we proceed as follows. In order to preserve the original geometry of the survey, we perform a random extraction of the galaxy coordinates weighted by the sum of the exposure maps of the 28 MAGG fields. The redshift of each mock galaxy is randomly extracted from a flat distribution limited to the range  $3.0 \leq z \leq 4.5$ . We require the size of the random sample to be a multiple of the number of real galaxies:  $N_{R,g} = \beta_g \times N_{D,g}$ . The factor  $\beta_g = 3$  is chosen as it is sufficient to populate the coordinates space and optimize the Poissonian fluctuations of the random sample.

We assemble the random sample of absorbers in a similar fashion. Lying on the line-of-sight, the three-dimensional position of each absorber is defined by the quasar coordinates and the redshift measured from the Voigt fit of the line. To preserve the geometry of the survey for the random sample of absorbers, we avoid the telluric bands and generate the redshift of the mock absorbers by randomly extracting values in the C iv redshift path. Given a number  $N_{D,a}$  of observed C iv systems, we build a sample of  $N_{R,a} = \beta_a \times N_{D,a}$  random absorbers, where  $\beta_a = 5$  to compensate for the smaller sample size.

#### 4.2.2 Galaxy auto-correlation

The galaxy auto-correlation function is derived by counting the number of real galaxies and random pairs in each bin in two dimension (transverse distance and line-of-sight separation). The intervals of transverse distances are logarithmically spaced between 0.05 – 0.50 pMpc, where the lower bound accounts for the typical resolved size of the emitters and the upper bound is set by the field di-

mension. Along the line of sight, we consider pairs with a separation  $5 \leq \Delta v/\text{km s}^{-1} \leq 2500$ , corresponding to  $0.02 \lesssim D_{\text{los}}/\text{Mpc} \lesssim 8.2$  at  $z = 3$ . To optimally extract the signal, the binned correlation function is oversampled and smoothed with a Gaussian filter of standard deviation  $\sigma = 5$ , corresponding to the oversampling factor. The result is shown in the left panel of Figure 8, up to a transverse distance  $R = 0.25$  pMpc to make it comparable with the galaxy-absorber cross-correlation function. A clear clustering signal is detected at a transverse distance  $R \lesssim 0.1$  pMpc and line-of-sight separation  $R_{\text{los}} \lesssim 0.1$  pMpc as expected for galaxy populations that are not randomly distributed in the Universe. A weaker clustering signal is elongated up to  $R_{\text{los}} \approx 0.5$  pMpc, likely due to the proper motions of the galaxies.

#### 4.2.3 Comparison with the galaxy-absorber cross-correlation

We use the same procedure employed for the galaxy auto-correlation function to derive the LAE-C iv correlation function in two dimensions, as a function of the transverse distance and the line-of-sight separation. Since the C iv absorbers are detected along the sightline to the central quasar in each field, we choose the interval 0.05 – 0.25 pMpc for the transverse separations, where the lower limit accounts for the quasar PSF and the upper limit corresponds to half the size of a field at  $z \approx 3.0$ . The line-of-sight separation between the LAEs and the C iv systems are derived by correcting the redshift of the galaxies for the observed offset from the absorbers,  $\Delta v \approx 246 \text{ km s}^{-1}$ . The cross-correlation function is shown in the right panel of Figure 8. At transverse distances  $R \lesssim 0.1$  pMpc and line-of-sight separations  $R_{\text{los}} \lesssim 0.5$  pMpc, that is at small separations from a C iv absorber, the probability to observe an LAE is enhanced with respect to a random point in the field, reinforcing the evidence that the LAEs are clustered to C iv absorbers on this scale. Both the galaxy auto-correlation and the galaxy-absorber cross-correlation functions are elongated in redshift space, possibly due to the galaxies proper motions and the gas proper motions relative to the galaxies, as it is typically observed in the literature ([Adelberger et al. 2003, 2005; Turner et al. 2014; Herrero Alonso et al. 2021](#)). In detail, [Turner et al. \(2014\)](#) performed a similar analysis measuring the optical depth as a tracer of metals in different ionization stages (e.g., H I, C iv O vi) around galaxies and found evidence of absorption enhancement extending up to  $\approx 180$  kpc in the transverse direction and on scales a factor  $\approx 5$  larger along the LOS.

A complete analysis involving the Cauchy-Schwarz relation would be possible by deriving the C iv absorbers auto-correlation function. In our survey, the absorption systems are observed along the line-of-sight of the central quasar of the MAGG fields which are separated by large transverse distances that exclude any possible physical correlation between the absorbers. Therefore, the C iv absorber auto-correlation function can only be computed in one-dimension as a function of the line-of-sight separation. The amplitude of the C iv absorbers auto-correlation function is almost flat with small fluctuations around  $\xi_{AA} \approx 0.0 - 0.2$  at any line-of-sight separation. This suggests that the clustering of C iv absorbers may be too weak to be observed with our sample since it collects a high number of absorption systems, but spread across a large redshift range and along 28 different sightlines. For this reason, we can only derive a  $3\sigma$  upper limit for the absorbers auto-correlation function that results in  $\xi_{AA} \lesssim 2.0$  at any line-of-sight separation in the range  $\Delta v = 200 - 2500 \text{ km s}^{-1}$  (the lower limit accounts for the rest frame separation of the C iv doublets and the median width of the lines), corresponding to  $R_{\text{los}} \approx 0.6 - 7.0$  pMpc.

The comparison between the LAEs auto-correlation with the

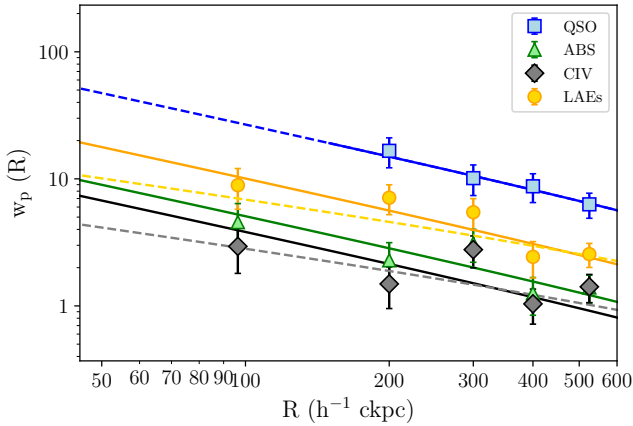


**Figure 9.** Reduced angular cross-correlation function for the LAEs associated to the C IV absorbers (black diamonds) with  $\gamma = 1.8$  (solid black line) and  $\gamma = 1.5$  (dotted black line) at  $S/N > 7$ . We compare this result with the ABS sample from MAGG IV (green triangles) and the QSO sample from Fossati et al. (2021) (blue squares), both of which are computed for  $S/N > 5$  and assuming  $\gamma = 1.8$ . The LAEs auto-correlation function (gold circles) is obtained by integrating the 2-dimensional function along the line-of-sight direction.

galaxy-absorber cross-correlation function can be used to test whether galaxies and C IV systems trace the same underlying matter distribution. Previously, Adelberger et al. (2003, 2005) detected metals around galaxies up to a transverse distance of  $\approx 300$  pkpc and found evidence of a clustering signal of C IV absorption systems near LBGs from the analysis of the galaxy-absorber cross-correlation function at  $z \sim 3$ . They used the analogies in the galaxy auto-correlation and the galaxy-absorber cross-correlation function as a hint to conclude that the galaxies and the absorption systems show a tight correlation and likely arise in the same regions of the Universe. However, a comparison between the LAEs auto-correlation and the galaxy-absorber cross-correlation suggests that the two functions do not show identical shapes nor the same amplitude in MAGG. Based on this result, we do not have direct evidence in support of the fact that LAEs and the C IV absorbers selected by MAGG are exclusively tracing the same regions of the Universe. It is of course possible that the C IV auto-correlation function at small line-of-sight separations combines with the galaxy auto-correlation function to yield the Cauchy-Schwarz equality, but we are fundamentally limited on measuring the C IV auto-correlation below few hundreds of  $\text{km s}^{-1}$ . Therefore, from this analysis, we can conclude that a correlation between the two populations is evident from what is shown so far, but there is no evidence that would exclude that at least a fraction of the C IV systems arise beyond the halos of LAEs, from other regions such as the IGM filaments.

#### 4.2.4 Radial extent of the LAE overdensity near C IV

As a complement to the analysis of the luminosity function, we now study the LAE-C IV clustering signal in terms of the reduced angular cross-correlation function, also comparing with different tracers of the LAE environment (C IV and H I absorbers, and quasars). As found before, the two-dimensional cross-correlation function is elongated in the line-of-sight direction (as seen in the right panel of Figure 8) due to the uncertainties in the redshift measurement via Ly $\alpha$  combined with the underlying peculiar velocities. Therefore, the line-

Sample	$r_0$ ( $\text{h}^{-1}$ cMpc)	$\gamma$
QSO	$3.58^{+0.34}_{-0.39}$	1.8
LAE	$2.07^{+0.23}_{-0.24}$	1.8
	$2.47^{+0.38}_{-0.40}$	1.5
ABS	$1.42^{+0.23}_{-0.27}$	1.8
C IV	$1.23^{+0.25}_{-0.27}$	1.8
	$1.39^{+0.32}_{-0.36}$	1.5

**Table 7.** Parameters of the best power-law function that reproduces the reduced angular cross-correlation function for the tracers studied in MAGG.

of-sight velocities are not an ideal measure of the radial distance for the galaxy-absorber cross-correlation. We thus focus next on the angular cross-correlation function,  $\omega_p(R)$ , as a function of the transverse distance  $R$  by integrating the original three-dimensional cross-correlation  $\xi(r) = (r/r_0)^\gamma$  over a small redshift window. To do so, we follow the method described in Trainor & Steidel (2012), also adding the results for the correlation functions derived in MAGG using the central quasars (Fossati et al. 2021) and the LLSs (MAGG IV) as tracers. The full description of this analysis is detailed in Fossati et al. (2021) and only briefly summarized below.

Our estimate of the angular cross-correlation function in the data is, consistent with what is adopted in other papers of the MAGG series, defined as the number of observed LAEs,  $N_{\text{obs}}$ , in excess with respect to the predicted number,  $N_{\text{pred}}$ :

$$\omega_p(R) = \frac{N_{\text{obs}}}{N_{\text{pred}}} - 1 \quad (3)$$

The estimator in Equation 3 requires a measure of the comoving mean density of LAEs in the fields. To derive this value, we first compute the number of LAEs within  $\pm 500 \text{ km s}^{-1}$  from a random redshift obtained from shuffling the real redshifts of the C IV absorbers observed in other fields. We then divide this number by the comoving area of the survey, assuming each field to be modeled as a square with 0.98 arcmin on a side. The measure and the relative uncertainty of  $n_{\text{pred}} = (35.16 \pm 6.94) \text{ h}^{-2} \text{ cMpc}^{-2}$  is derived by bootstrapping the C IV redshift with random extractions over  $10^3$  repetitions and by taking the 16th and 84th percentiles. Finally, the expected number of galaxies in each interval of distance is derived by multiplying the mean density of galaxies in the fields,  $n_{\text{pred}}$  by the comoving area of the circular annulus corresponding to the  $i$ -th radial bin:  $N_{\text{pred}} = n_{\text{pred}} \pi (R_{i+1}^2 - R_i^2)$ .

The results are shown as black dots in Figure 9 with the respective uncertainties and summarized in Table 7. Due to the central quasar PSF contamination, we mask the region at distances  $R < 2$  arcsec corresponding to  $R \lesssim 43 \text{ h}^{-1} \text{ cMpc}$  at redshift  $z \approx 3.0$ . The solid and dashed black lines are a fit to the projected correlation function with free parameter  $r_0$ . Due to the degeneracy of the two parameters  $r_0$  and  $\gamma$ , we fix the slope of the power law, and study the implication of this assumption by choosing two different values  $\gamma = 1.8$  (Hennawi et al. 2006; Bielby et al. 2011; Diener et al. 2017; García-Vergara et al. 2017, 2019) and  $\gamma = 1.5$  (Trainor & Steidel 2012). Consistently with what Trainor & Steidel (2012) pointed out, we observe that the correlation length decreases with increasing slope of the power law from  $r_0 = 1.39^{+0.32}_{-0.36} \text{ h}^{-1} \text{ cMpc}$  for  $\gamma = 1.5$  to  $r_0 = 1.23^{+0.25}_{-0.27} \text{ h}^{-1} \text{ cMpc}$  for  $\gamma = 1.8$ . Despite the model suggesting that a positive correlation extends towards the edge of the MUSE field of view, at distances  $R \gtrsim 400 \text{ h}^{-1} \text{ cMpc}$  the larger uncertainties make the number of LAEs at larger separation from the C IV absorbers consistent with expected field number.

The observed LAEs overdensity at small distances from the C IV absorbers is compared in Figure 9 with the excess of LAEs observed

in the surroundings of the central quasars of each field (Fossati et al. 2021) and the LLSs from MAGG IV. Differently from the connection criteria adopted by Fossati et al. (2021), in order to perform a consistent comparison, we restrict the QSO sample to the LAEs at  $S/N > 5$  observed at line-of-sight separations within  $\pm 500 \text{ km s}^{-1}$  from the quasars (which is half the window in the original analysis). To do this, we correct the LAE mean density from Fossati et al. (2021) as  $n_{\text{LAE,pres}}^{\text{QSO}} = 0.5 (17.15 \pm 2.28) = (8.58 \pm 1.14) \text{ h}^{-2} \text{ Mpc}^{-2}$ . For the C iv and H I MAGG samples, the region at distances  $R < 50 \text{ h}^{-1} \text{ ckpc}$  is masked due to contamination of the central quasars PSF. The only exception is represented by the MAGG QSO sample, for which the masked region is extended to  $R < 150 \text{ h}^{-1} \text{ ckpc}$ . In this case, the behaviour of the correlation function on smaller scales is an extrapolation from the best-fit power law (dashed blue line in Figure 9). In the entire MUSE FoV, the correlation length with respect to quasars is  $r_0 = 3.58^{+0.34}_{-0.39} \text{ h}^{-1} \text{ cMpc}$ , which is higher than it is around the LLSs,  $r_0 = 1.42^{+0.23}_{-0.27} \text{ h}^{-1} \text{ cMpc}$ , and the C iv absorbers,  $r_0 = 1.23^{+0.25}_{-0.27} \text{ h}^{-1} \text{ cMpc}$ .

A similar analysis has been performed to study the radial profile of C iv absorption around LBGs. Adelberger et al. (2003, 2005) selected C iv absorbers with column densities  $N_{\text{C iv}} \gtrsim 10^{12.5} \text{ cm}^{-2}$  (corresponding to a rest-frame equivalent width  $W_r \approx 0.01 \text{ \AA}$ , of the same order of magnitude as the 50% completeness limit of this work sample) and derived a C iv-LBGs cross-correlation length that is a factor  $\approx 2.2$  larger than what we measured for the LAEs in our sample, assuming a power-law slope  $\gamma = 1.8$ . Adopting a different approach, Turner et al. (2014) produced 2D optical depth map showing that metal absorption is enhanced at small transverse separations from  $z \approx 2 - 4$  galaxies. A significant excess of C iv absorption is also observed near LAEs at higher redshift  $z \gtrsim 3$ . Muzahid et al. (2021) recovered C iv optical depth profiles by stacking lines in the spectra of 8 bright quasars and found a significant enhancement of C iv absorption within  $\approx 500 \text{ km s}^{-1}$  and  $\approx 250 \text{ kpc}$  from 96 LAEs at  $z \approx 3.3$ .

To complete the analysis, we derive the projected LAEs auto-correlation function by integrating the two-dimensional function shown in Figure 8 along the line-of-sight direction up to a separation of  $500 \text{ km s}^{-1}$ . Uncertainties are derived by applying a bootstrap procedure over the assembly of the random galaxy sample. Following the same strategy we applied for the other MAGG tracers, we measure the correlation length from a power-law modelling of the projected function for fixed slopes. The resulting LAEs correlation length  $r_0 = 2.07^{+0.23}_{-0.24} \text{ h}^{-1} \text{ cMpc}$  for  $\gamma = 1.8$  (and  $r_0 = 2.47^{+0.38}_{-0.40} \text{ h}^{-1} \text{ cMpc}$  for  $\gamma = 1.5$ ) is a factor  $\approx 1.5$  and  $\approx 1.7$  larger compared to that obtained for the H I and C iv sampled, respectively and  $\approx 1.7$  times lower compared to that obtained for LAEs clustering around quasars. Our estimate of the LAEs correlation length is found to be consistent, within the uncertainties, with the values measured in the literature for LAEs at redshift  $z \sim 3$  (corrected for the cosmology adopted in this paper):  $r_0 = 2.5^{+0.6}_{-0.7} \text{ h}^{-1} \text{ cMpc}$  (Gawiser et al. 2007),  $r_0 = 1.78^{+0.41}_{-0.48} \text{ h}^{-1} \text{ cMpc}$  (Ouchi et al. 2010) and  $r_0 = 2.99^{+0.35}_{-0.35} \text{ h}^{-1} \text{ cMpc}$  (Bielby et al. 2016). We also observe that our result is consistent with the correlation length measured by Herrero Alonso et al. (2021) for a sample of  $\approx 700$  LAEs at redshift  $3 < z < 6$ . At first, they optimized the  $k$ -estimator to measure the LAE clustering for a survey with large redshift range, but limited angular coverage, and measured  $r_0 = 3.76^{+3.24}_{-0.94} \text{ h}^{-1} \text{ cMpc}$  and  $\gamma = 1.3^{+0.36}_{-0.45}$ . However, employing a more traditional method, they modelled the projected two-point correlation function with a

power law and measured  $r_0 = 2.34^{+0.26}_{-0.37} \text{ h}^{-1} \text{ cMpc}$  with a slope  $\gamma = 1.85^{+0.25}_{-0.25}$  that appears to fully agree with our findings.

Altogether, the analysis of the correlation functions, of the luminosity function and of the excess of LAEs in velocity space, provide firm evidence that LAEs cluster differently around the various tracers found across the entire MUSE FoV. The strongest signal is found near quasars and the amplitude of the clustering decreases progressively for LLSs and then for the C iv absorbers. While LLSs and C iv absorbers show a comparable level of clustering as expected for an overlapping population (43/220 of the C iv selected in this work are in fact associated with the LLSs from MAGG IV), there is a sufficient evidence for an excess of LAEs around LLSs compared to C iv, suggesting that high-column density H I absorbers are more prominently associated to the (outer) CGM of halos compared to the C iv absorbers with  $\gtrsim 0.08 \text{ \AA}$ , which are more likely to also trace gas at larger distances from LAEs.

### 4.3 Covering fraction of ionized gas

In the previous sections, we explored the existence of a physical association between the C iv absorbers and the LAEs using an *absorber-centered* approach and searching for galaxies in their surroundings. Carrying on the analysis of the connection between C iv absorbers and LAEs with a statistical method, we now turn to a *galaxy-centered* point of view. To avoid proximity effects, we masked all the LAEs observed within a LOS separation  $|\Delta v| \leq 3000 \text{ km s}^{-1}$  from the redshift of the central quasar of each field. We thus derive the C iv covering fraction as a function of the transverse distance in order to measure the observed occurrence of C iv absorbers around the LAEs. The covering fraction is defined as the number of LAEs connected to a C iv absorber (according to the above definition, i.e. within a  $500 \text{ km s}^{-1}$  window centred on the peak seen in Figure 6) with rest-frame equivalent width above a given threshold  $W_r^{1548} \geq W_0$ , relative to the total number of LAEs lying in the C iv redshift path:

$$f_c(R) = \frac{N_{\text{obs}}(R; W_r^{1548} \geq W_0)}{N_{\text{tot}}(R)}. \quad (4)$$

In Figure 10 we show the differential covering fraction derived in radial annuli (first panel), and thus including LAEs with transverse distances in the  $i$ -th interval  $R_i < R < R_{i+1}$ , and the cumulative covering fraction, at radial separations  $R < R_{i+1}$  (second panel). The vertical error bars account for the  $1\sigma = 68\%$  Wilson-score confidence intervals, while in the left panel the horizontal bars reproduce the width of each radial interval. The covering fraction is computed for three rest-frame equivalent width thresholds ( $0.05, 0.10, 0.30$ )  $\text{ \AA}$ . As expected from the frequency distribution function, the C iv covering fraction decreases with increasing threshold from  $f_c \approx 80\%$  with  $W_0 = 0.05 \text{ \AA}$ , to  $f_c \approx 50\%$  with  $W_0 = 0.10 \text{ \AA}$  and  $f_c \approx 35\%$  with  $W_0 = 0.30 \text{ \AA}$  at  $R \lesssim 50 \text{ kpc}$ . For each C iv equivalent width threshold, the covering fraction decreases with increasing transverse separation between LAEs and the connected absorbers from  $f_c \approx 60\%$  at  $R < 100 \text{ kpc}$  with  $W_0 = 0.05 \text{ \AA}$  to  $f_c \approx 50\%$  at  $R > 100 \text{ kpc}$ . For the strongest C iv absorbers in the sample, assuming a threshold  $W_0 = 0.30 \text{ \AA}$ , the covering fraction is smaller at any transverse separation and decreases from  $f_c \approx 30\%$  at  $R < 100 \text{ kpc}$  to  $f_c \approx 20\%$  at  $R > 100 \text{ kpc}$ . We also observe that the differential covering fraction (first panel in Figure 10) increases in outer radial interval ( $R > 200 \text{ kpc}$ ). Although it is not statistically significant, Dutta et al. (2020) observed a similar trend studying Mg II absorbers at lower redshift and explained it as possibly due to the superposition of individual galaxy halos in case of multiple galaxies associated

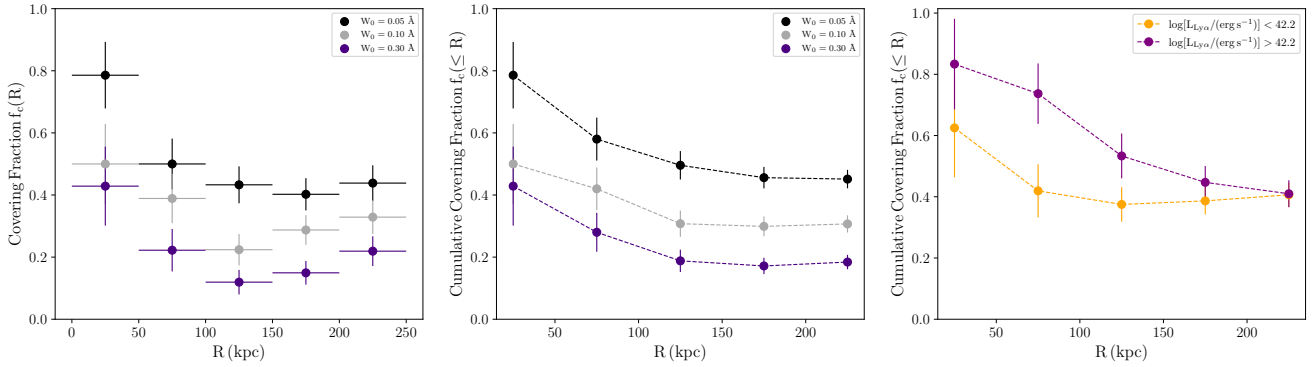


**Figure 10.** Differential (first panel) and cumulative (second panel) covering fraction,  $f_c(R)$ , as a function of the projected distance from the line-of-sight assuming three different equivalent width limits (see legend). The vertical error bars reproduce the  $1\sigma$  Wilson-score confidence interval, while horizontal error bars in the left panel mark the width of each radial bin. The third panel shows the cumulative covering fraction dividing the LAEs in two bins of  $\text{Ly}\alpha$  luminosity, assuming an equivalent width threshold  $W_0 = 0.05 \text{ \AA}$ .

with the same C IV system. In the end, the observed trend suggests that the probability to observe a C IV within  $\pm 500 \text{ km s}^{-1}$  of an LAE is enhanced at small transverse separations and decreases at higher distances roughly up to  $R \approx 100 \text{ kpc}$  before flattening. Hence, C IV is present around LAEs on scales that extend well beyond the virial radius, which typically measures  $R_{\text{vir}} \approx 25 - 53 \text{ kpc}$  for halo mass of the order of  $M_h \approx 10^{10} - 10^{11} M_\odot$  (Herrero Alonso et al. 2021) respectively.

Similar trends as a function of the transverse separation and the absorption strength are observed in the literature (Bordoloi et al. 2014; Turner et al. 2014; Burchett et al. 2016; Rudie et al. 2019; Dutta et al. 2021). In particular, Bordoloi et al. (2014) derived the covering fraction at  $z < 0.1$  for C IV absorbers detected up to  $\approx 100 \text{ kpc}$ . They measure, at transverse separations of  $R < 50 \text{ kpc}$ ,  $f_c \approx 73\%$  for C IV absorber with  $W_r > 0.1 \text{ \AA}$  and  $f_c \approx 36\%$  for  $W_r > 0.3 \text{ \AA}$ . Both these results are consistent within  $1\sigma$  with our findings at  $R < 50 \text{ kpc}$  for the same equivalent width thresholds. At higher redshift,  $z \sim 2.0$ , Rudie et al. (2019) derived the covering fraction by computing the fraction of LBGs with a C IV system within line-of-sight separation up to  $1000 \text{ km s}^{-1}$  and within a transverse separation  $100 \text{ kpc}$ . The covering fraction decreases from  $f_c \approx 50\%$  to  $f_c \approx 33\%$  for increasing column density threshold from  $\log(N_0 / \text{cm}^{-2}) = 13.0^2$ . This result is consistent at  $1\sigma$  with the fraction of LAEs for which we detect C IV absorption above the threshold  $W_0 = 0.05 \text{ \AA}$  within a similar transverse separation  $R < 100 \text{ kpc}$ . Using a large sample of galaxies up to redshift  $z \approx 1.5 - 1.6$ , Dutta et al. (2021) measured a C IV covering factor beyond  $200 \text{ kpc}$  of around  $40\%$  for  $W_0 = 0.03 \text{ \AA}$  which is just  $25\%$  below our determination for  $W_0 = 0.05 \text{ \AA}$  at comparable distances. Thus, comparing with our MAGG survey, the analysis of the C IV covering fraction over  $\approx 10 \text{ Gyr}$  of cosmic time could potentially imply small evolution with redshift, which appears to be driven by the lowest equivalent width systems.

In order to study whether the incidence of C IV absorbers depends on the properties of the galaxies, we derive the cumulative covering fraction for a threshold of  $W_0 = 0.05 \text{ \AA}$  in two bins of  $\text{Ly}\alpha$  luminosity above and below  $\log(L_{\text{Ly}\alpha,0} / \text{erg s}^{-1}) = 42.2$  (see the third panel in Figure 10). We find that the fraction of C IV within  $\pm 500 \text{ km s}^{-1}$  of LAEs is enhanced up to  $f_c \approx 80\%$  for luminous galaxies relative to  $f_c \approx 63\%$  for the fainter LAEs within transverse separation  $R < 50 \text{ kpc}$ . The covering fraction decreases to  $f_c \approx 75\%$

and  $f_c \approx 41\%$  at higher separations  $R < 100 \text{ kpc}$  for the two galaxies population, respectively, before flattening at  $f_c \lesssim 50\%$  and  $f_c \lesssim 40\%$  for distances  $R > 100 \text{ kpc}$ . A larger covering factor around LAEs with higher SFR (assuming  $\text{Ly}\alpha$  as a proxy of star formation activity) is in line with what is observed for Mg II at  $z \approx 1$  by Dutta et al. (2020) in MAGG and by Dutta et al. (2021) at  $z < 2$  in QSAGE survey. As for lower redshift, however, it is difficult to discern whether this difference arises because of the different star formation or whether – assuming LAEs lie on the star formation main sequence – it is a mere reflection of the different size of the halos probed as a function of  $\text{Ly}\alpha$  luminosity. Additional information, and in particular independent mass estimates from IR observations, are required to investigate this trend further.

#### 4.4 Detailed analysis of the C IV-LAE associations

Since the link between the C IV absorption-line systems and LAEs encodes useful information about the enrichment of the CGM, we now explore the possible correlations between the properties of the ionized gas and those of the galaxies. The upper panels in Figure 11 show the absorbers’ rest-frame equivalent width and velocity width as a function of the  $\text{Ly}\alpha$  luminosity of the associated galaxies. Here, we divide the LAEs in two sub-samples based on a threshold on the  $\text{Ly}\alpha$  luminosity ( $L_{\text{Ly}\alpha} = 10^{42.2} \text{ erg s}^{-1}$ ) and we compare the resulting distributions to highlight any intrinsic difference in the two sub-populations. For those C IV absorbers that are not connected to any LAEs within  $\pm 500 \text{ km s}^{-1}$ , we take an upper-limit corresponding to the  $\text{Ly}\alpha$  luminosity at which our search is  $10\%$  complete. The brightest LAE of each group is considered in the analysis.

In the upper-left panel in Figure 11 we observe that the distribution of the equivalent width of the C IV absorbers not connected to a galaxy reveals that a higher number of systems is weak (with  $W_r \lesssim 0.05 \text{ \AA}$ ) compared to those with LAEs detected, and drops off at larger equivalent widths. The equivalent width distribution of the absorbers connected to bright LAEs is significantly skewed toward stronger systems with  $W_r \gtrsim 0.1 \text{ \AA}$ , suggesting that the strongest absorbers show a preference to be connected to luminous galaxies. Weak C IV systems with  $W_r \lesssim 0.02 \text{ \AA}$  are completely absent in this more luminous sub-sample. To quantify the statistical difference among these distributions, we perform a Kolmogorov–Smirnov test and derive the probability that the  $W_r$  distribution of C IV absorbers with no associated LAEs and that of C IV absorbers connected to bright ( $L_{\text{Ly}\alpha} > 10^{42.2} \text{ erg s}^{-1}$ )

<sup>2</sup>  $W_0 = 0.05 \text{ \AA}$  corresponds to approximately  $\log(N_0 / \text{cm}^{-2}) = 13.5$ .

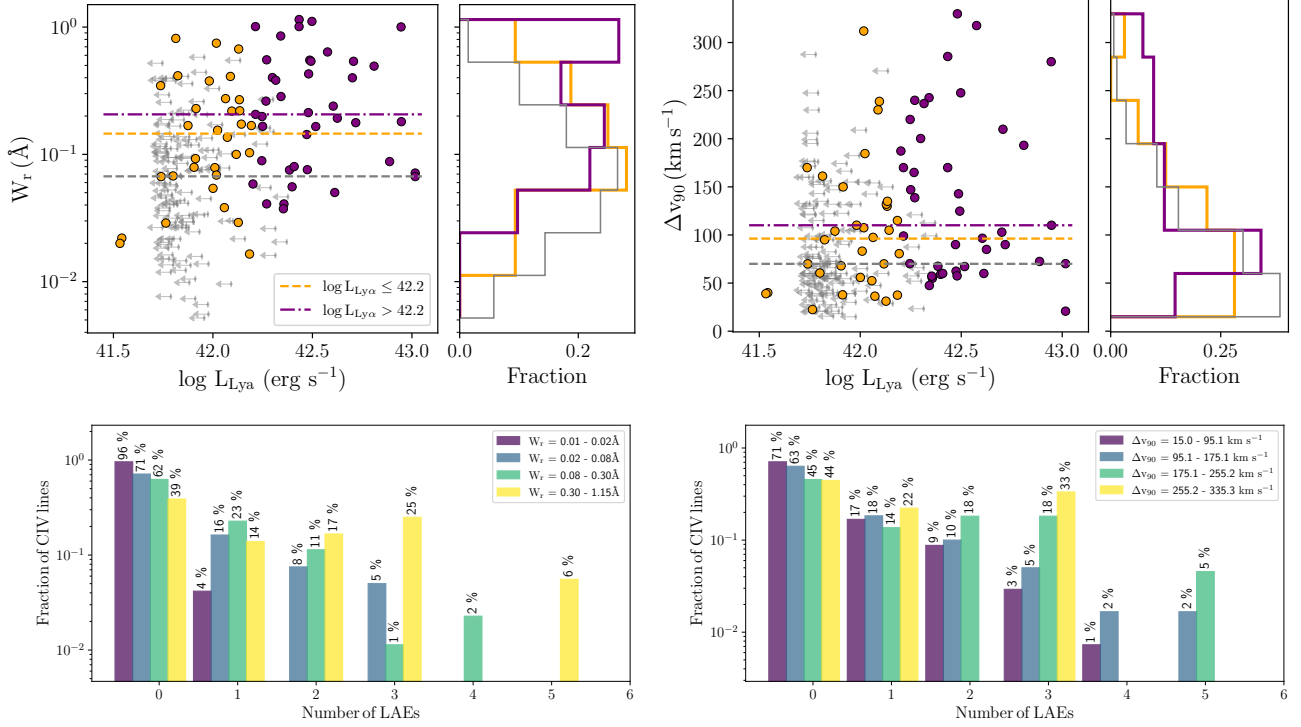


**Figure 11.** Upper panels: C IV absorbers’ equivalent width (left) and velocity width (right) as a function of the Ly $\alpha$  luminosity of the galaxies found within  $\pm 500$  km s<sup>-1</sup>, divided in two sub-samples below (orange) and above (purple) a threshold of  $L_{Ly\alpha} = 10^{42.2}$  erg s<sup>-1</sup>. Dashed lines mark the median of each distribution, shown as histograms along the right hand-side axis. The grey arrows mark instead the Ly $\alpha$  luminosity upper-limit for the C IV systems without any associated LAE. Lower panels: distribution of the equivalent width (left) and velocity width (right) as a function of the number of galaxies connected to each absorber.

Samples	$W_r$ (Å)	$\Delta v_{90}$ (km s <sup>-1</sup> )
Bright LAEs - Faint LAEs	0.22	0.12
Bright LAEs - LAE non-detections	$5.12 \times 10^{-5}$	$4.20 \times 10^{-3}$
Faint LAEs - LAE non-detections	0.01	0.22

**Table 8.**  $p$ -values resulting from the KS test that measures the probability that the distribution of C IV properties for different Ly $\alpha$  luminosity of the associated galaxy is drawn from the same parent distribution.

or faint ( $L_{Ly\alpha} \leq 10^{42.2}$  erg s<sup>-1</sup>) LAEs are drawn from the same parent distribution. The results, shown in Table 8, corroborate on statistical grounds the observation of stronger C IV absorbers being connected to brighter galaxies. Likewise, C IV absorbers that are not connected to any galaxy within  $\pm 500$  km s<sup>-1</sup> are weaker, with large significance, than those associated to faint LAEs. However, we also note the distribution for the absorbers with no associated LAEs is not limited to the weakest systems, but extends up to  $W_r \approx 1.0$  Å covering the full range of equivalent-width we measured. LAEs connected to these strong absorbers may not be detected because they are outside the MUSE FOV or they may be heavily obscured by dust.

A similar analysis, focusing instead on the C IV velocity width, is presented in the second panel of Figure 11. Here, comparing the two sub-samples, we find that the LAE non-detections are mostly limited to the narrowest C IV systems with  $\Delta v_{90} \leq 100$  km s<sup>-1</sup> with a sharp drop-off at  $\Delta v_{90} \geq 200$  km s<sup>-1</sup>. The distribution of the velocity width of the C IV absorbers connected to bright LAEs shows a tail extending at  $\Delta v_{90} \geq 150$  km s<sup>-1</sup> relative to those associated to less luminous galaxies. In Table 8 we show the  $p$ -values resulting from the KS test, which again support on statistical grounds the differences observed between the two samples.

Finally, in the lower panels of Figure 11 we investigate the C IV absorbers equivalent width (left figure) and velocity width (right figure) as a function of the number of associated LAEs within  $\pm 500$  km s<sup>-1</sup>. To do so, we divide the absorbers into 4 intervals of  $W_r$  and  $\Delta v_{90}$ . We derive the fraction of C IV absorbers connected to a certain number of LAEs and with equivalent-width (velocity width) in a certain range, over the total number of systems with  $W_r$  ( $\Delta v_{90}$ ) in that interval. The bottom-left panel of Figure 11 supports the existence of a marked correlation between the strength of the C IV absorption and the number of connected galaxies. We do not detect any LAE at close separation from the  $\approx 96\%$  of the weakest absorbers with  $W_r \leq 0.02$  Å, while the remaining  $\approx 4\%$  is connected to isolated galaxies. Conversely,  $\approx 48\%$  of the strongest absorbers ( $W_r \geq 0.3$  Å) are found to be associated with  $\geq 2$  LAEs, with the few rich groups hosting 4 and 5 galaxies being found exclusively near high equivalent width C IV absorbers.

The same analysis is then repeated for the absorbers’ velocity width in the bottom right panel of Figure 11. In this case, we do not find a correlation that is as significant as above. Indeed, we do not observe any LAE in the vicinity of  $\approx 71\%$  of the narrow systems with  $\Delta v_{90} \leq 95$  km s<sup>-1</sup>, but  $\approx 13\%$  of them are connected to  $\geq 2$  galaxies. However,  $\approx 44\%$  of the broadest systems with  $\Delta v_{90} \geq 255$  km s<sup>-1</sup> are not associated with any LAE,  $\approx 22\%$  is found in proximity to 1 galaxy. Only  $\approx 33\%$  of this sample is connected to 3 LAEs. A significant fraction of both narrow and wide absorbers,  $\approx 19\%$  of the systems with  $\Delta v_{90} \sim 95 - 175$  km s<sup>-1</sup> and  $\approx 41\%$  with  $\Delta v_{90} \sim 175 - 255$  km s<sup>-1</sup>, is associated to  $\geq 2$  galaxies.

In conclusion, splitting the sample of C IV-LAE associations below and above the galaxies luminosity  $L_{Ly\alpha} = 10^{42.2}$  erg s<sup>-1</sup> reveals that

the C IV absorbers found within  $\pm 500 \text{ km s}^{-1}$  from a bright galaxy are on average stronger and more kinematically complex compared to the systems connected to faint galaxies or without any LAE detected in the field-of-view. A high fraction ( $\approx 44\%$ ) of the strongest absorbers with  $W_r \geq 0.30 \text{ \AA}$  is found to be connected to  $\geq 2$  galaxies and the number of associated LAEs decreases with decreasing equivalent width. The same analysis applied to the absorbers velocity width revealed no such clear correlation, with only the  $\approx 33\%$  of broad systems with  $\Delta v_{90} \geq 255 \text{ km s}^{-1}$  connected to multiple galaxies.

#### 4.4.1 Radial profile of the C IV absorption strength

To complete the picture of the distribution of the ionized gas around LAEs, we turn to investigate how the rest-frame equivalent width depends on the projected distance from the galaxy associated to each C IV absorber. The results for C IV are shown in the left panel of Figure 12.

Many studies in the literature support the evidence of an anti-correlation between the rest-frame equivalent width of the C IV absorbers and the transverse separation from the associated galaxy. Most of these are focused on galaxies at low redshift  $z \lesssim 1$  (Chen et al. 2001; Bordoloi et al. 2014; Burchett et al. 2016) and  $z \sim 1 - 1.5$  (Dutta et al. 2021). Similar results are observed for LBGs at higher redshift  $z \sim 2 - 3$  with a statistical approach based on spectral stacking and optical depth analysis (Steidel et al. 2010; Turner et al. 2014). Motivated by these findings, we search for an anti-correlation following the procedure described by Dutta et al. (2020) and briefly summarized here. The rest-frame equivalent width is expected to decrease with increasing distance from the associated galaxies following a log-linear relation that models an expected steep decrease of the strength of the absorption regulated by a scale factor that is linked to the galaxy virial radius:

$$\log(W_r / \text{\AA}) = a + b \cdot (R / \text{kpc}). \quad (5)$$

For those LAEs that lie in C IV redshift path, but that are not connected to any C IV absorber within  $\pm 500 \text{ km s}^{-1}$ , we derive a  $3\sigma$  upper limit (arrows in Figure 12). We fit the full sample with the function in Eq. 5 applying a Bayesian method based on a likelihood that takes both measurements and upper limits into account (see for more details and applications Chen et al. 2010; Rubin et al. 2018; Dutta et al. 2020, 2021). The result is shown in Figure 12 as solid black line, where the shaded grey region marks the  $1\sigma$  confidence interval. We notice that the modelling is strongly driven by the upper limits at large distances where a significant fraction of the data is scattered upward the relation and the equivalent width profile appears to be flatter.

Dutta et al. (2021) performed a similar analysis on 123 C IV absorption-line systems at lower redshift,  $z \sim 0.1 - 2.4$ . The best log-linear model resulting from their fit is shifted significantly upward compared to the one derived in this work and parametrized by  $a = -0.42^{+0.25}_{-0.28}$  and  $b = -0.002^{+0.001}_{-0.001}$ . The QSAGE (Bielby et al. 2019; Stott et al. 2020) dataset explored by Dutta et al. (2021) results in a  $3\sigma$  sensitivity limit of  $W_r^{\text{C IV}} \approx 0.1 \text{ \AA}$  for the detection of C IV absorbers, dominated by the measurements based on UV spectra with a lower resolution and S/N compared to the optical spectra available in MAGG. In this work, the upper limits at transverse distances  $R \lesssim 100 \text{ kpc}$ , that are absent in the sample from Dutta et al. (2021), follows from the higher resolution of the MAGG spectra and pushes down the fit towards lower equivalent width values. Moreover, the size of the field-of-view at low redshift is about a factor of  $\approx 2$  larger than it is at high redshift, making it possible to detect galaxies up to transverse separations  $R \approx 750 \text{ kpc}$ , far beyond the typical virial

radius of a dark matter halo with  $M_H \approx 10^{11} M_\odot$ . Extending the analysis to larger distances lead to a fit that is flatter compared to the one at high redshift. Thus, the differences in the two datasets make it difficult to directly compare our findings with low redshift results and explain the discrepancies as due to a physical evolution with redshift. We note, however, that detections occupy a comparable region of parameter space, all clustering between  $0.1 - 1 \text{ \AA}$ .

#### 4.5 Dependence on galaxy environment

The ability of MUSE observations to obtain a complete survey inside the FoV reveals that a large fraction of the observed galaxies are part of a group (see Sect. 3.4 for the definition and identification of groups), allowing us to study the multiphase circumgalactic gas as a function of galaxy environment (see e.g. Bielby et al. 2017; Fossati et al. 2019; Muzahid et al. 2021; Dutta et al. 2021).

In Figure 12, we distinguish between isolated galaxies (red) and groups (blue), considering only the closest galaxy of each group, and we place an equivalent width upper-limit at  $3\sigma$  for the LAEs that are detected in the C IV redshift path, but are not associated to any absorber within  $\pm 500 \text{ km s}^{-1}$  (arrows). An excess of galaxies in groups, relative to the number of isolated LAEs, is observed at small transverse separations for  $R \lesssim 60 \text{ kpc}$ . The observed C IV absorbers connected to groups show, on average, a rest-frame equivalent width that is  $\approx 2.5$  times larger than that associated to isolated galaxies at any separation, consistent with the trend shown in third panel in Figure 11. This difference is suppressed approaching the edges of the field-of-view at  $R \geq 200 \text{ kpc}$ . Galaxies without C IV absorption detected within  $\pm 500 \text{ km s}^{-1}$  are mostly found at large distances ( $R \geq 100 \text{ kpc}$ ) from the sightlines. We recall that our classification of isolated galaxies and groups is limited by the size of the FoV and thus it is not possible to know if an isolated galaxy, especially those connected to strong absorbers, does not have any companion outside the observed footprint.

Next, we derive the differential and cumulative covering fraction for the isolated LAEs (to the completeness limit of our survey) and the galaxies that are part of a group (i.e. with at least a companion within  $\pm 500 \text{ km s}^{-1}$  and within the MUSE FoV). The results are shown Figure 13 for the full sample of galaxies in groups (first column) and for sub-samples assembled including only the closest or the brightest component of each group (second and third columns respectively). The cumulative covering fraction of isolated and group galaxies decreases with increasing transverse distance and flattens above  $R > 100 \text{ kpc}$ . We observe, however, that the fraction of galaxies in groups with detected C IV absorption within  $\pm 500 \text{ km s}^{-1}$  is on average a factor  $\approx 3$  higher relative to the fraction of isolated galaxies for any transverse separation up to  $R \approx 250 \text{ kpc}$ .

Our result is, at small separations, consistent with the findings from Dutta et al. (2021) at  $z < 2$  on a sample of  $\approx 750$  galaxies detected in MAGG and QSAGE. Indeed, their analysis revealed that the covering fraction of C IV absorbers around group galaxies is a factor  $\approx 2$  higher relative to that of the isolated galaxies up to  $R < 100 \text{ kpc}$ . In their analysis, the difference is less pronounced than in our sample for larger impact parameters, where we observe a persistent difference up to the edge of the FoV. Exploiting the large spectral coverage of MAGG and QSAGE, they also compared the covering fraction of the intermediate ionized gas phase, traced by the C IV absorbers, with that of a low ionized phase traced by the Mg II absorption, both for groups and isolated galaxies, finding that the covering fraction is enhanced by a factor  $\approx 2 - 3$  for the Mg II gas in group galaxies. A substantial difference is, however, observed once control samples are built for the isolated galaxies by requiring them to match the impact



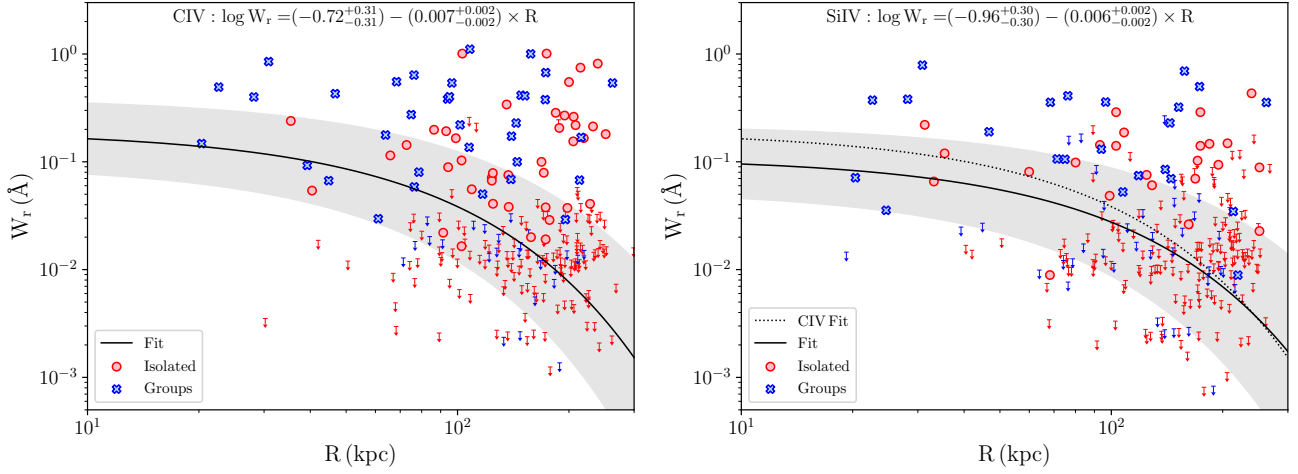


**Figure 12.** Rest-frame equivalent width as a function of the transverse separation from the associated galaxies for the C iv (left panel) and the Si iv (right panel) absorbers. The isolated LAEs are shown in red, while the closest galaxy of a group is shown in blue. For the galaxies without any associated absorber we derive a  $3\sigma$  upper limit (arrows with the same color-coding). The observed relationship is fitted with a log-linear function taking upper limits into account. The best fit result is drawn as a solid black line and the  $1\sigma$  uncertainties are marked by shaded regions. In the right panel, the best fit obtained for the Si iv absorbers (solid line) is compared to the best fit derived for the C iv (dotted line).

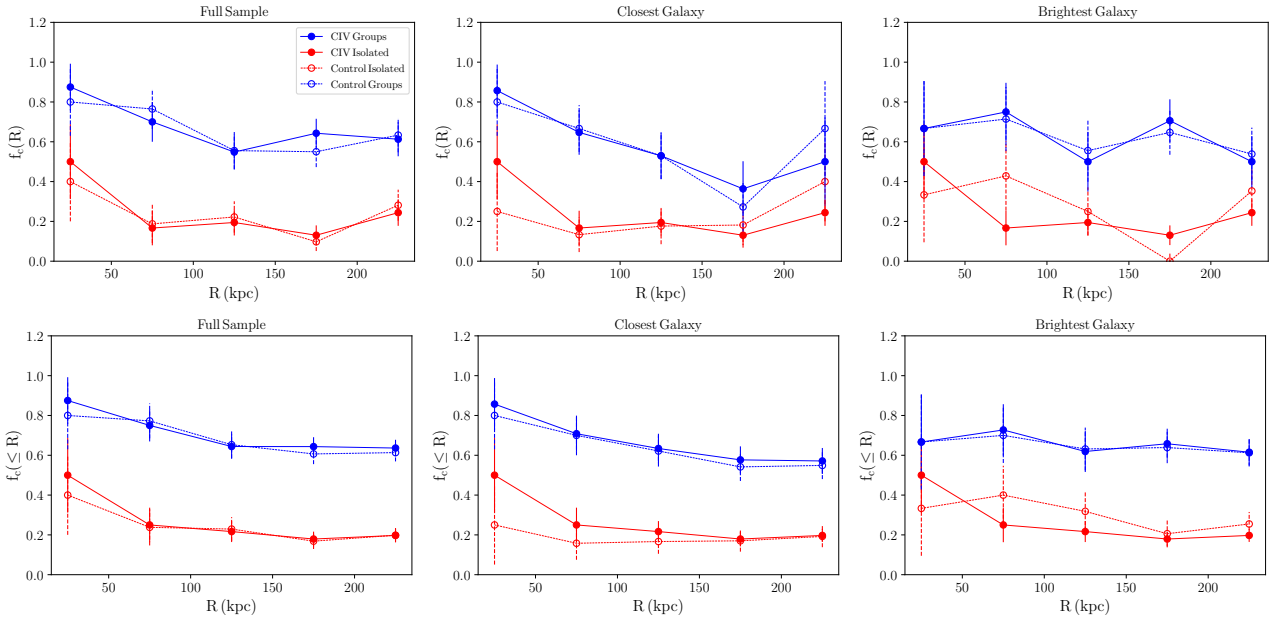


**Figure 13.** Differential (top row) and cumulative (bottom row) covering fraction of C iv around isolated galaxies and galaxies in groups that are connected to C iv absorbers within  $\pm 500 \text{ km s}^{-1}$ , as a function of the transverse separation. All the galaxies in groups are considered in the *Full Sample*. The analysis is reproduced by taking only the closest (second column) and the brightest (third column) component of each group. These measurements (solid lines) are compared to the covering fraction estimated for control samples (dashed lines) assembled by requiring the properties of isolated galaxies and groups to match.

parameter, the stellar mass and the redshift of the galaxies in groups. For these control samples, the enhancement of the covering fraction in group galaxies relative to that of the isolated galaxies is preserved only for the Mg II absorption, but it is suppressed for the C iv gas.

In light of this result, we define a control sample to study in detail whether the excess in covering factor of group galaxies is an intrinsic property or depends on the properties of the sample. We build control-matched samples from groups by selecting the members of the groups with properties resembling those of the isolated galaxies. Specifically, we select group galaxies within  $\pm 20 \text{ kpc}$  from the impact parameter and  $\pm 0.15 \text{ dex}$  from the log of the Ly $\alpha$  luminosity of the

isolated LAEs, without allowing for repetitions. The same strategy is then applied to assemble a control sample of isolated galaxies. The result is shown in Figure 13 (blue and red dashed line for groups and isolated galaxies, respectively). In order to test the quality of the control samples, we perform a KS test comparing the properties of the control samples to the ones of groups and isolated galaxies and measure a  $p$ -value  $> 0.95$  for all the cases shown in Figure 13. In building these control samples, we notice (see Table 9) that isolated galaxies and groups do not differ significantly in their properties, but stronger differences are observed only if considering the closest or the brightest component of each group. In these cases, we assem-

Property	Isolated	Groups	Groups (R)	Groups (L)
LAEs in C IV redshift path				
$R$ (kpc)	163.54	169.42	128.45	162.88
$\log[L_{\text{Ly}\alpha}/(\text{erg s}^{-1})]$	42.12	42.08	42.07	42.20
LAEs with C IV within $\pm 500 \text{ km s}^{-1}$				
$R$ (kpc)	168.62	168.41	105.53	168.10
$\log[L_{\text{Ly}\alpha}/(\text{erg s}^{-1})]$	42.20	42.03	41.97	42.13

**Table 9.** Median properties of LAEs in the C IV redshift path (rows 1 – 2) and of LAEs with C IV absorbers detected within  $\pm 500 \text{ km s}^{-1}$  (rows 3 – 4). Columns 4 – 5 are referred to the samples containing only the closest (R) and the brightest galaxy (L) of each group respectively.

bly control samples of groups and isolated galaxies with the same strategy described above to reproduce the properties of the isolated sample and of the closest or the brightest component of each group respectively. The results are shown in the middle and right panels in Figure 13. The comparison to the covering fraction of group galaxies (blue-dashed line) and that of the isolated galaxies (red-dashed line) in matched samples show that the enhancement in groups is preserved for the control samples.

A similar study on the effect of environment was also conducted by Muzahid et al. (2021) who performed a statistical analysis on the strength of C IV absorption along the line of sight based on spectral stacking. In line with our findings, they report a stronger C IV absorption connected to galaxies in groups, relative to those observed in the vicinity of isolated galaxies, up to velocities of a few hundreds km/s. These authors interpret the observed excess as a consequence of galaxies being embedded in a large-scale structure which give rise to the C IV absorption, and not simply due to the properties of the two samples which appear comparable (see their table 4).

#### 4.6 Comparison with Si IV as a tracer

The analysis presented in the previous sections has focused on C IV as tracer of moderately ionized and possibly warm gas. An alternative tracer of gas in the same ionization stage that is accessible for observation with MAGG spectroscopy is the Si IV doublet, which has a slightly lower but overall comparable ionization potential ( $\approx 45.1 \text{ eV}$  for Si IV and  $\approx 64.5 \text{ eV}$  for C IV). Making use of the detection of both C IV and Si IV absorption-line systems in MAGG, we now test explicitly whether differences in the correlation between Si IV and LAEs exist in comparison to C IV (arising, for instance, from differences in the nucleosynthesis or the shape of the ionizing spectrum), or whether the results presented above largely apply for Si IV as well. The latter scenario would support the hypothesis that C IV and Si IV absorbers are both tracers of the same gas phase in the CGM or IGM. To this end, we derive the galaxies luminosity and cross-correlation functions of LAEs and Si IV systems in comparison with what is found with C IV. We perform a blind search of LAEs within  $\pm 500 \text{ km s}^{-1}$  from a Si IV absorber with the same procedure adopted for the C IV analysis. We find that 49 Si IV absorbers are connected to 86 LAEs, corresponding to a detection rate of  $46 \pm 8$  per cent (49/108) that is a factor  $\approx 1.4$  higher compared to the C IV detection rate but still consistent within  $1\sigma$  uncertainty. Once we identified the LAEs associated to Si IV absorbers, we compute the LAE luminosity function and the projected cross-correlation to measure the amplitude and the radial profile of the galaxy overdensity. The results are shown in Figure 14. We find that the luminosity function of LAEs around Si IV absorbers is modelled by a Schechter function whose best-fit parameters are the characteristic luminosity

$\log[L^*/(\text{erg s}^{-1})] = 42.645 \pm 0.273$ , slope  $\alpha = -1.466 \pm 0.370$  and normalization  $\log[\phi^*/(\text{Mpc}^{-3} \text{ dex}^{-1})] = -2.058 \pm 0.431$ . These estimates are all consistent with the C IV results within  $1\sigma$  uncertainties. Furthermore, the projected cross-correlation function is modelled by a power law with correlation length  $r_0 = 1.48^{+0.29}_{-0.32} \text{ h}^{-1} \text{ cMpc}$  assuming a slope  $\gamma = 1.8$  and increases to  $r_0 = 1.71^{+0.40}_{-0.42} \text{ h}^{-1} \text{ cMpc}$  for  $\gamma = 1.5$ . All these parameters are consistent within  $1\sigma$  with the results derived for the C IV-LAE cross-correlation.

Complementary to this empirical analysis, we further support these findings by adopting a more theoretical approach, detailed in Appendix A, to show that C IV and Si IV absorbers likely arise from the same gas.

In conclusion, this analysis provides evidence that the C IV and Si IV systems are comparable tracers of ionized gas, and that the results obtained in studying the galaxy overdensity around these absorption-line systems are not strongly sensitive to the tracer adopted.

## 5 DISCUSSION

### 5.1 Properties of C IV absorbers near galaxies as a function of mass and redshift

#### 5.1.1 Comparison of the MAGG and MUSEQuBES samples

Following the pioneering survey by Adelberger et al. (2003, 2005), several studies have reported evidence of metal enrichment in the form of C IV in the CGM of star-forming galaxies at the mass scale traced by  $z \approx 2 - 3$  LBGs ( $M_H \approx 10^{12} M_\odot$ ; Steidel et al. 2010; Turner et al. 2014; Rudie et al. 2019). Only recently, this analysis has been extended to the lower-mass galaxy population traced by LAEs at  $z \approx 3$ , with  $M_H \approx 10^{11} M_\odot$ . Besides MAGG, the other major survey that studies the distribution of C IV near LAEs is MUSEQuBES (Muzahid et al. 2021). By observing samples of LAEs at comparable redshift and sensitivity to our study, these authors followed a complementary approach to ours by stacking quasar spectra at the wavelength of H I and C IV near 96 LAEs at redshift  $2.9 < z < 3.8$ . Through this technique, they observe an excess of H I and C IV absorption within a line-of-sight separation  $\Delta v \leq \pm 500 \text{ km s}^{-1}$ , i.e., on comparable scales to the velocity clustering seen in MAGG (Figure 6). Consistently with the covering fraction shown in Figure 10, the excess of C IV absorption is extended at large projected distances ( $R \geq 250 \text{ kpc}$ ), corresponding to  $R \approx 7 R_{\text{vir}}$  for halo masses  $M_H \approx 10^{11} M_\odot$  with virial radius  $R_{\text{vir}} \approx 35 \text{ kpc}$ . However, through stacking, Muzahid et al. (2021) report no evident difference in the line-of-sight optical depth at different impact parameters, while our detailed analysis of the equivalent width as a function of impact parameter suggests a mild decline in the absorption strength as one moves away from galaxies. Compared to the results by Muzahid et al. (2021), MAGG data reveal a higher fraction of stronger absorbers near brighter LAEs. This observation hints at a correlation between SFR and C IV equivalent width, that is only observed in MUSE-QuBES in H I. We note, however, that Muzahid et al. (2021) rely on rest-frame UV continuum emission for measuring SFRs, while we use Ly $\alpha$  emission.

These authors also report that the C IV absorbing gas shows a strong dependence as a function of the different galaxy environments connected to the absorbers. In their sample,  $\approx 33\%$  of the LAEs are in groups (i.e., not isolated within  $\pm 500 \text{ km s}^{-1}$ ) and this fraction is even higher ( $\approx 44\%$ ) in the MAGG sample. They found that both H I and C IV absorption are enhanced around galaxies in groups with respect to the isolated LAEs. According to our estimate of the

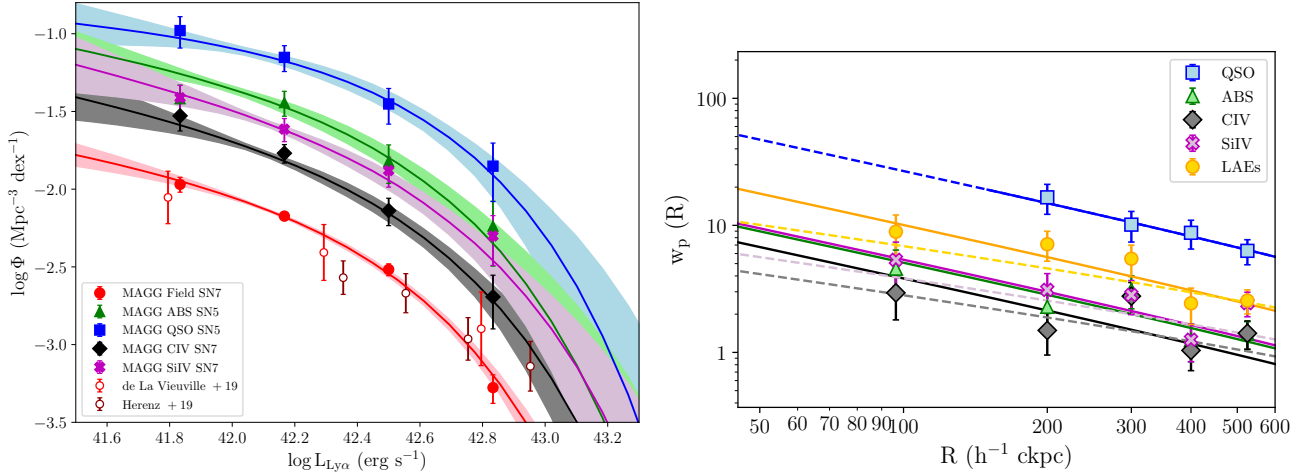


**Figure 14.** Measure of the amplitude and the radial profile of the LAEs overdensity observed within  $\pm 500 \text{ km s}^{-1}$  from Si iv absorbers using the luminosity function (left panel, purple markers) and the projected cross-correlation (right panel, purple markers). Markers and color-coding are the same as Figures 7 and 10, respectively, for the other tracers studied in MAGG.

covering fractions (Figure 13), the C iv absorbers are preferentially detected around groups rather than isolated galaxies, at least up to the edges of the field of view. Furthermore, they observe that the H I absorption is stronger and broader in groups, but the weakness of the C iv absorption prevents from deriving a significant difference between isolated galaxies and groups. The larger size of the MAGG sample allows us to detect, on average,  $\approx 2.5$  times stronger and  $\approx 1.5$  times broader C iv absorbers around groups compared to those around isolated galaxies, suggesting that the galaxy environment does also affect the strength of the absorption and, to a lesser extent, the kinematics of the gas.

In summary, the study of both the MAGG and MUSEQuBES samples lead to mostly similar conclusions with independent data and different analysis techniques: there is clear clustering of LAEs and C iv absorbers on scales up to  $\pm 500 \text{ km s}^{-1}$  along the line of sight and  $\approx 200 \text{ kpc}$  in the transfer direction, and the environment appears to modulate this signal. Owing to the study of individual associations, MAGG adds further insight into this analysis, unveiling stronger/wider C iv absorption near brighter LAEs, and a correspondence between the strongest absorbers and the presence of groups. Finally, by studying the LAE population near absorbers (and not the strength of absorption near LAEs), we confirm that only a small fraction of C iv is in fact associated to galaxies ( $\approx 36 \pm 5$  per cent) and this fraction increases with the strength of the absorption.

### 5.1.2 Comparison of MAGG galaxies and $z \approx 2 - 3$ LBGs

Many studies in literature have shown there is a physical connection between continuum detected galaxies with the surrounding ionized gas detected in absorption in background quasars or galaxy pairs (Turner et al. 2014; Bordoloi et al. 2014; Burchett et al. 2016; D’Odorico et al. 2016; Rudie et al. 2019; Schroetter et al. 2021). Compared to LBGs, our study extends this investigation to LAEs at  $z \approx 3 - 4$  in lower-mass halos ( $M_H \approx 10^{11} M_\odot$ ). We now investigate analogies or differences between these two galaxy populations and the properties of the ionized and enriched gas around them.

Considering first galaxies alone, Bielby et al. (2016) offer a direct comparison between LAEs and LBGs using data from the VLT Lyman break galaxies (LBG) redshift survey. From their measurement of the LAEs correlation length,  $r_0 = (2.99 \pm 0.35) h^{-1} \text{cMpc}$ , they

derive a halo mass  $M_H = 10^{11 \pm 0.3} M_\odot$ , which is lower compared to the typical values measured for LBGs,  $r_0 \approx 4.18 h^{-1} \text{cMpc}$  and  $M_H \approx 10^{12} M_\odot$  (Adelberger et al. 2005; Bielby et al. 2011). However, the correlation length of the two population are found to be consistent at the fainter magnitudes, suggesting that LAEs inhabit on average low-mass haloes but that the two populations are overlapping (see, e.g., Steidel et al. 2011). Thus, statistics of C iv near LAEs and LBGs are not independent.

Turning to the association between C iv and LBGs, Adelberger et al. (2003, 2005) studied the spatial distribution of the ionized gas by means of the galaxy auto-correlation,  $\xi_{\text{gg}}$ , and the galaxy-absorbers cross-correlation,  $\xi_{\text{ga}}$ , functions. Modeling the two-point correlation functions as a power law with a slope  $\gamma_{\text{ga}} \approx 1.6$ , their measurement of the cross-correlation length  $r_{\text{ga}} \approx 3.34 h^{-1} \text{cMpc}$  is a factor  $\approx 2.4$  higher compared to the value  $r_0 \approx 1.39 h^{-1} \text{cMpc}$  estimated for LAEs, assuming a fixed slope  $\gamma = 1.5$ , and a factor  $\approx 2.7$  higher compared to the estimate  $r_0 \approx 1.23 h^{-1} \text{cMpc}$  with a fixed slope  $\gamma = 1.8$  (Figure 9). They also found that the shape of the galaxy-absorber cross-correlation is consistent with the galaxy auto-correlation down to C iv systems with column density  $N_{\text{CIV}} \gtrsim 10^{12.5} \text{cm}^{-2}$  suggesting that LBGs and C iv absorbers inhabit similar regions of the Universe. However, this is not completely the case for the sample of LAEs and C iv systems studied in this work. As mentioned above, our results (Figure 8) show that the galaxy auto-correlation and the galaxy-absorbers two dimensional cross-correlation functions have different shapes and amplitudes, suggesting that the LAEs and the ionized C iv gas are unlikely to trace exclusively the same underlying matter distribution and thus, do not always inhabit the same regions.

The enhancement of C iv absorption around LBGs is also observed by Turner et al. (2014), who adopted the optical depth method to measure the absorption strength and produce 2D maps of the average distribution of metal absorption around these galaxies. These maps reveal a strong enhancement of metal absorption at small transverse separations from the galaxies at  $R \lesssim 180 \text{ kpc}$ , which is elongated in the LOS direction up to  $\Delta v \lesssim \pm 240 \text{ km s}^{-1}$  ( $\approx 1 \text{ Mpc}$ ) due to the gas peculiar motions.

The analysis performed on larger scales suggests that the C iv absorbing gas is typically extended far beyond the virial radius of LBGs, generalizing the finding of Rudie et al. (2019) who measured

the covering fraction of strong ( $N \geq 10^{13.5} \text{ cm}^{-2}$ ) C IV systems to reach a value  $f_c \approx 50\%$  up to  $R \approx 100 \text{ kpc}$ , that is  $\approx R_{\text{vir}}$ . Indeed, Turner et al. (2014) detected C IV absorption up to the survey limit ( $\approx 2 \text{ Mpc}$ ) in the transverse direction, corresponding to  $\approx 20 R_{\text{vir}}$  for an average halo mass  $M_{\text{H}} \approx 10^{12} M_{\odot}$ . The C IV absorbing gas shows a similar tendency to be extended far beyond the typical virial radius ( $R_{\text{vir}} \approx 25 - 35 \text{ kpc}$  for halo mass  $M_{\text{H}} \approx 10^{10} - 10^{11} M_{\odot}$  respectively) also around LAEs. The covering fraction in Figure 10 shows that  $\approx 50\%$  of the LAEs are connected to C IV absorbers within  $\pm 500 \text{ km s}^{-1}$  at  $R > 100 \text{ kpc}$ , reaching as far as the survey limit of  $R \approx 250 \text{ kpc}$  which corresponds to  $\approx 10 R_{\text{vir}}$ .

As the separation between the ionized and enriched gas and the associated LBGs approaches the virial radius, the strength of the absorption is commonly observed to decrease monotonically with increasing distance. The spectral stack performed by Steidel et al. (2010) shows a steep decrease of the rest-frame equivalent width of strong absorbers (with  $W_r \geq 0.1 \text{ \AA}$ ) up to the galaxy virial radius, which can be extrapolated leading to a sharp drop-off at larger distances. Considering weaker absorption, Turner et al. (2014) showed that the equivalent width decreases more slowly with the transverse separation relative to the predictions from Steidel et al. (2010) and flattens around  $W_r \approx 0.1 \text{ \AA}$  at  $R > 100 \text{ kpc}$ , up to the edges of their survey.

Turning to the LAEs population at  $z \sim 3$ , Muzahid et al. (2021) observed that the absorption strength as a function of the transverse distance, normalized by the virial radius, is at the level found near LBGs by Turner et al. (2014), but without any significant monotonic decrease. In Figure 12, the log-linear modeling of the equivalent width as a function of the distance shows that the absorption strength decreases at  $R \gtrsim 30 \text{ kpc}$ , corresponding to the typical virial radius in which LAEs reside. However, this trend is strongly driven by the non-detections, with measured values remaining somewhat flat between  $0.1 - 1 \text{ \AA}$  also beyond  $\approx 100 \text{ kpc}$ .

In this context, Hasan et al. (2021) studied the statistical distribution of C IV gas relative to different galaxy populations and its evolution across the redshift range  $0 \leq z \leq 5$  by means of an absorption model. Their model predicts that all the C IV absorbers are confined within the virial radius of low mass halos, while weak systems with  $W_r \geq 0.05 \text{ \AA}$  may live beyond the virial radius of the most massive galaxies at redshift  $z > 2.5$ . These predictions are consistent with the observed extension of C IV gas around massive galaxies, with strong  $W_r \geq 0.3 \text{ \AA}$  absorbers detected in the inner regions of the CGM and the weakest systems spread at distances larger than the virial radius. However, the model does not reproduce the large extension of weak and strong C IV absorbing gas around low mass haloes that host LAEs. A possible explanation may reside in the assumptions the model is based on, i.e. each individual C IV absorption line system is co-spatial with a single halo that hosts a single galaxy. We found that  $\approx 20\%$  of the C IV absorbers in our sample are connected to a multiple galaxies within  $\pm 500 \text{ km s}^{-1}$ . Given the limited size of the FoV, it is also possible that isolated galaxies have companions at larger separations. Thus, the galaxy environment might play a role in shaping the differences between the observed and predicted C IV extension around low mass galaxies.

Altogether, this comparison highlights how both LAEs and LBGs coexist with a significant distribution of C IV gas which is clearly associated to the galaxy themselves on small scales, but that appears more weakly correlated as one moves to larger distances and lower equivalent widths.

### 5.1.3 Comparison with lower redshift results

The MAGG survey has been also employed to investigate the properties of the cool gas, probed by Mg II absorption, around galaxies at  $z \sim 0.8 - 1.5$  (Dutta et al. 2020) for which the authors infer solar masses of  $M_{\star} \approx 10^9 M_{\odot}$ . Moreover, they combined results with the QSAGE survey, to trace both the more neutral and ionized gas phases around galaxies through Mg II and C IV absorption at  $z < 2$  (Dutta et al. 2021). Their findings allow us to compare the properties of the cooler Mg II gas with the more ionized C IV gas both at low and high redshift.

At  $z < 2$ , the strength of the absorption is found to decrease with increasing distance. The anti-correlation is steeper for the Mg II absorbers compared to the C IV gas. However, the radial profile of both the Mg II and C IV absorption strength shows a significant scatter and flattening once galaxies in groups are included in the analysis (see also Bordoloi et al. 2011; Fossati et al. 2019), with strong absorption detected even at large transverse separations around groups. This is consistent with our findings shown in Figure 12, where the anti-correlation is sensitive to the upper limits, but strong systems are observed at any separations. A direct comparison as a function of redshift is made difficult by the different size of the FoV and the different sensitivities of these surveys. However, a general trend appears: a significant contribution to the flattening in the  $W_r - R$  relation of C IV absorbers may come at all redshift from the larger extension of the highly-ionized gas which, as argued at lower redshift (Dutta et al. 2021), is possibly embedding the cooler phase. Similar results are indeed found around LBGs at  $z \sim 2$  by Rudie et al. (2019), with singly-ionized ions commonly detected at smaller distances from the galaxies relative to higher ionization species.

Finally, the galaxy environment is observed to play an important role in shaping the properties of the absorbers both at low and high redshift. At  $z \lesssim 2$ , the Mg II systems connected to multiple galaxies are  $\approx 5$  times stronger and show a  $\approx 3$  times higher covering fraction up to  $R \approx 200 \text{ kpc}$  ( $\sim 2 R_{\text{vir}}$ ) compared to those associated to isolated galaxies. Fossati et al. (2019) found stronger Mg II absorption around 4 groups at redshift  $z \sim 0.5 - 1.5$  and invoked gravitational interactions between the components of a group as a possible mechanism responsible for the enhanced Mg II absorption. Moreover, Dutta et al. (2021) found that the C IV covering fraction, both connected to groups and isolated galaxies, is  $\approx 2$  times higher relative to Mg II systems, and enhanced in groups up to  $R \approx 750 \text{ kpc}$  ( $\approx 5 R_{\text{vir}}$ ). However, once a control sample of isolated galaxies is assembled to reproduce the properties of the groups, the excess is still significant for Mg II absorbers, but is suppressed for the C IV systems. In contrast, at  $z \gtrsim 3$  (Figure 13), we notice that the C IV covering fraction of control samples of galaxies in groups is confidently detected to be higher compared to isolated galaxies. Our findings are also supported by similar results from Muzahid et al. (2021). Therefore, there seems to be a hint of a possible redshift evolution in how more neutral and ionized gas phases respond to different galaxy environments. However, the C IV sample at  $z < 2$  suffers from more limited statistics compared to  $z \approx 3$ . Likewise, there is currently no systematic study of the Mg II distribution near  $z \approx 3$  LAEs. This evolution scenario should therefore be tested further with better spectroscopic coverage for C IV at  $z < 2$  and for Mg II at  $z \gtrsim 3$ . The latter effort is the objective of an ongoing X-Shooter campaign (PID 0109.A-0559; PI M. Galbiati).

## 5.2 C iv and H I around $z > 3$ LAEs

As a complement to the analysis presented here for ionized gas traced by C iv absorbers around LAEs, in the MAGG IV paper we have studied the link between these galaxies and the neutral gas traced by optically-thick absorption line systems. The MAGG IV sample is a collection of 61 strong H I absorbers ( $N_{\text{HI}} \gtrsim 10^{16.5} \text{ cm}^{-2}$ ),  $\approx 84$  per cent of which are associated to 127 LAEs within  $\pm 1000 \text{ km s}^{-1}$  at redshift  $z \approx 2.9 - 4.2$ . Reducing the velocity separation to the limit we chose to associate absorbing gas and galaxies to the one adopted in this work, 45 H I absorbers are connected to 97 LAEs within  $\pm 500 \text{ km s}^{-1}$  centered on the peak of the velocity separation distribution (found at  $\Delta v \approx 250 \text{ km s}^{-1}$  in MAGG IV). These numbers correspond to an LAE detection rate of  $\approx 74 \pm 15$  per cent around H I gas, a factor  $\approx 2$  higher relative to the fraction of C iv systems connected to at least one galaxy within the same velocity window.

Searching for the presence of metal absorption-lines as a probe of the metallicity of H I systems, in MAGG IV we identify a sample of 58 C iv absorbers that have been analysed independently from this work. Of these C iv absorbers, excluding upper limits for non detections and systems falling within telluric regions (5/58), we found that all these absorbers have a counterpart in the sample assembled in this work within a redshift separation  $\Delta z = 0.0045$  ( $\Delta v \approx 300 \text{ km s}^{-1}$  at  $z = 3.5$ ) with  $\approx 81$  per cent (43/53) detected at  $W_r^{1550} > 3\sigma$ . We observe that  $\approx 51$  per cent (22/43) of these systems are connected to at least 1 galaxy, with  $\approx 33$  per cent (14/43) connected to galaxies that are part of a group. Based on this different detection rate, we conclude that if LLSs trace both the CGM and the filaments connecting several LAEs as argued in MAGG IV, C iv absorbers only partially trace these same structures. This conclusion is reinforced by the statistical estimates of the LAE luminosity function (Figure 7) and the galaxy-absorber cross-correlation function (Figure 9). Our analysis shows that the LAE number density is higher around strong H I absorbers relative to C iv systems both as a function of the galaxy luminosity and the transverse separation, indicating a stronger connection between strong H I and LAEs than between C iv and LAEs.

### 5.2.1 The role of cosmic filaments

We investigate whether differences exist between the full sample of C iv absorbers relative to the sub-samples of C iv systems that are connected to strong H I systems or not. The results are shown in the upper panels of Figure 15, while the  $p$ -values resulting from a KS test are listed in Table 10. We observe a lack of weak ( $W_r \leq 0.01 \text{ \AA}$ ) C iv systems from MAGG IV and a small excess of strong absorbers  $W_r \gtrsim 0.1 \text{ \AA}$ , with  $\approx 40\%$  of the  $W_r \gtrsim 0.1 \text{ \AA}$  C iv systems included in this work connected to strong H I absorbers within  $\pm 500 \text{ km s}^{-1}$ . This suggests that the C iv systems connected to H I absorbers are, on average, a factor  $\approx 3.7$  stronger compared to the C iv that is not associated to H I absorbing gas. The KS test suggests that the systems with H I detection, compared to those without H I absorption and the full C iv sample, show an equivalent width that is unlikely to be drawn from the same parent distribution, with  $p$ -value  $< 10^{-6}$  and  $p$ -value  $< 10^{-4}$  respectively. On the other hand, the strength of the C iv absorbers without H I detection is more similar to that of the full C iv sample ( $p$ -value  $> 0.46$ ). The proximity to H I absorbers seems to affect also the kinematics of the gas, since the C iv systems have a velocity width that is a factor  $\approx 2.3$  broader if connected to H I absorbing gas. As found before, the KS test suggests that the  $\Delta v_{90}$  of the C iv absorbers with H I detection, compared to C iv without H I absorption and the full C iv sample, are unlikely to be drawn from the same parent population ( $p$ -value  $< 10^{-5}$  and

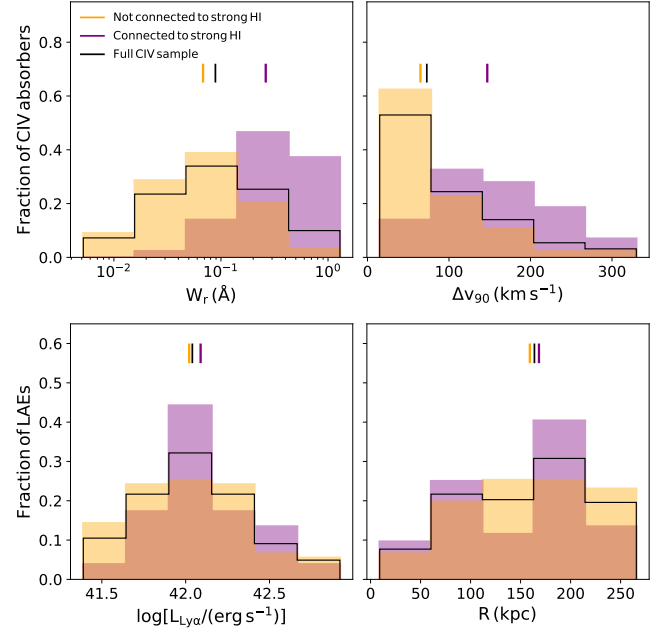


**Figure 15.** Upper panels: comparison between the distribution of the rest-frame equivalent width (left panel) and velocity width (right panel) of the full C iv sample (black) with the sub-sample overlapping MAGG IV catalogue (purple) and the remaining systems (orange). Lower panels: same as above, but comparing the Ly $\alpha$  luminosity (left panel) and the transverse separation (right panel) of the LAEs associated to the different C iv samples. Median values are shown as ticks.

$p$ -value  $< 10^{-3}$  respectively). C iv absorbers without H I detection do not significantly deviate ( $p$ -value  $> 0.57$ ) from the full C iv sample.

A similar analysis is performed to compare the transverse separation and the Ly $\alpha$  luminosity of the LAEs connected to the full C iv sample and to the systems that are or are not associated to H I absorbers. From the results shown in the lower panels of Figure 15, we notice that the C iv systems are associated to the population of LAEs that does not show any difference ( $p$ -value  $> 0.50$ ) in the Ly $\alpha$  luminosity they emit and in their transverse separation from the absorbing gas. Thus, this comparison suggests that C iv systems matched to strong H I absorbers have higher equivalent widths and are more broad kinematically, but this change in absorption properties does not influence significantly the emission properties of the associated LAEs. As mentioned above, MAGG IV results support the picture in which LAEs are clustered within large scale structures and strong H I absorbers are tracers of both the galaxies CGM and of the dense optically thick gas contained in the filaments connecting LAEs.

We have shown so far that strong C iv systems are connected to H I absorbers, suggesting that these systems might be tracers of the same large-scale structure as high-density neutral hydrogen. In support of this hypothesis, we would expect the galaxies to be aligned with respect to the positions of the C iv absorbers, similarly to what found when analysing strong H I absorbers (see MAGG IV). We thus follow the procedure adopted in MAGG IV and measure the offset between the galaxy positions and the axis connecting the C iv absorbers to the closest LAE. Only the 38 C iv systems connected to 2 or more LAEs are included in this analysis. Results are shown in Figure 16 as a function of C iv equivalent width threshold,  $W_0$ . We found an

Samples	$W_r$ (Å)	$\Delta v_{90}$ (km s $^{-1}$ )	$\log[L_{Ly\alpha}/(\text{erg s}^{-1})]$	$R$ (kpc)
With H I - Without H I	$8.69 \times 10^{-6}$	$1.12 \times 10^{-5}$	0.52	0.90
With H I - Full Sample	$1.52 \times 10^{-4}$	$6.59 \times 10^{-3}$	0.66	0.87
Without H I - Full Sample	0.46	0.57	>0.99	>0.99

**Table 10.** Results of KS test ( $p$ -values) that measures the probability that the distribution of C IV and LAEs properties (equivalent width, velocity width, LAE luminosity, impact parameter) for systems that are (With H I) and are not (Without H I), connected to strong H I absorbers are drawn from the same parent population.

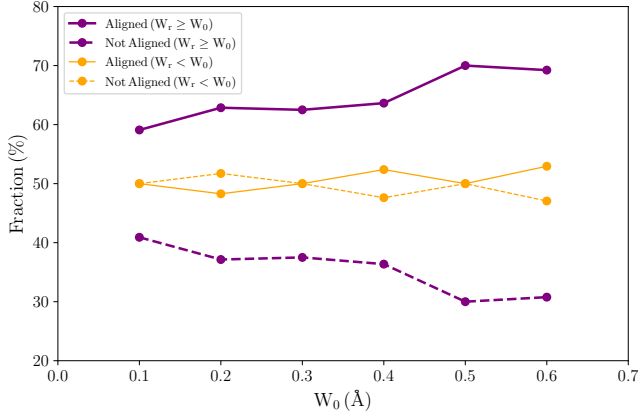


**Figure 16.** Fraction of LAEs aligned ( $0^\circ - 45^\circ$  or  $135^\circ - 180^\circ$ , solid line) and not aligned ( $45^\circ - 135^\circ$ , dashed lines) with the axis defined by the absorber and the closest LAE, as a function of the absorbers equivalent width. We show results for LAEs connected to  $W_{CIV} \geq W_0$  and  $W_{CIV} < W_0$  as purple and orange lines, respectively.

excess of aligned ( $< 45^\circ$  and  $> 135^\circ$ ) LAEs connected to strong ( $W_r \geq W_0$ ) C IV absorbers. The fraction of aligned LAEs increases with increasing absorption strength, while LAEs connected to weaker C IV ( $W_r < W_0$ ) does not show any preference to be aligned with the absorbers.

While strong C IV absorbers appear to overlap at least in part with optically-thick H I gas, the above analysis suggest that weaker C IV systems are tracer of a more homogeneous medium, found also at larger distances from galaxies where the H I column density is expected to decline (Rudie et al. 2012). We thus investigate if there is any difference in the average H I profiles associated with different ‘types’ of C IV absorbers. To do so, we stacked the Ly $\alpha$ , Ly $\beta$ , Ly $\gamma$  and Ly $\delta$  absorption at the redshift of each C IV system (where data were available) and compare the results we obtained for strong C IV absorbers ( $W_r \geq 0.1$  Å), weak C IV absorbers ( $W_r < 0.1$  Å) connected to at least one LAE and weak C IV absorbers that are not connected to any galaxies within  $\pm 500$  km s $^{-1}$ . The result is shown in Figure 17 and suggests that strong C IV absorbers arise from higher column density regions, likely close to the spine of the cosmic filaments where both galaxies and optically-thick absorbers reside (see MAGG IV), while weaker absorbers arise from lower column density regions away from the central parts of the filaments, where the presence of galaxies is more stochastic. Figure 17 further hints at a progressive less significant hydrogen absorption in weak C IV systems far from galaxies compared to a similar population of metal absorbers near LAEs.

In force of this analysis, we propose a new picture of the distribution of metals around LAEs in which strong C IV absorbers, as well as H I absorbers, trace dense regions of the filaments connecting galaxies. On the contrary, weaker C IV absorbers seem to lie progres-

sively farther from the galaxies and hence farther from the densest regions of the filaments, pinpointing to the existence of an enriched, but more diffuse and homogeneous medium that degrades towards the IGM.

### 5.2.2 The role of outflows

A variety of models has been studied in the literature in order to understand the physical processes that lead to the C IV enrichment of the CGM and IGM, spanning from Population III stars at high redshift ( $z \sim 25 - 30$ ), to more recent ejections of galactic winds and feedback powered by star formation activity in galaxies at  $z \sim 3 - 10$  (e.g. Simcoe et al. 2004). The C IV absorbers we observe at redshift  $z \sim 3 - 4$  may be the result of cumulative feedback processes that occurred at higher redshift and ongoing feedback ejections at the epoch near the peak of the star formation rate density towards  $z \approx 2$ .

We attempt to disentangle these two effects by exploring if it is plausible that the bulk of outflows powered by recent star formation in galaxies has instantaneously enriched all the observed absorption systems near LAEs. To this end, in Figure 18 we compare the transverse separation between the LAEs and the C IV absorbers found within  $\pm 500$  km s $^{-1}$  with the distance traveled by outflows, assuming they are launched at redshifts between  $z = 4$  and  $z = 6.5$  with steps  $\Delta z = 0.5$  and travel at average velocities  $< v > = 100, 250$  km s $^{-1}$  (solid and dashed lines respectively). We found that to reach C IV absorbers at separations  $R \geq 150$  kpc, outflows must be launched at redshift  $z \geq 6.5$  if travelling at  $< v > = 100$  km s $^{-1}$ , and are thus linked to episodes of star formation that happened in the galaxies  $\Delta t \geq 1$  Gyr before the epoch of observations. Outflows launched  $\Delta t \lesssim 750$  Myr before the observations and linked to more recent star formation activity in the galaxies must instead travel at average velocities  $< v > \geq 250$  km s $^{-1}$  to reach the C IV absorbers up to the edge of the FoV ( $R \approx 250$  kpc).

In a similar analysis, Díaz et al. (2021) interpreted the connection between 11 C IV absorbers and LAEs at  $z > 4.7$  as potentially due to the relatively recent ( $\Delta t \lesssim 700$  Myr at  $z \approx 5$ ) galaxy activity, modelled as outflows started at  $z = 10$  and travelling at average velocities  $< v > \leq 400$  km s $^{-1}$  for 89% (8/9) of the LAE sample. This scenario suggests that only outflows traveling at average high velocities ( $< v > \geq 250$  km s $^{-1}$ ) are able to enrich the gas around a fraction of the LAEs if powered by recent ( $\Delta t \lesssim 500$  Myr) star formation activity in galaxies.

## 6 SUMMARY AND CONCLUSIONS

In this work, we explored the connection between an ionized gas phase, traced by absorption-line systems in quasar spectra, and a population of Ly $\alpha$  emitting galaxies identified in the MUSE Analysis of Gas Around Galaxies (MAGG) survey, which combines medium-deep VLT/MUSE observations of 28 quasar fields with high S/N and high resolution spectroscopy of the central sources. We traced the ionized gas by assembling a sample of 220 C IV and 108 Si IV

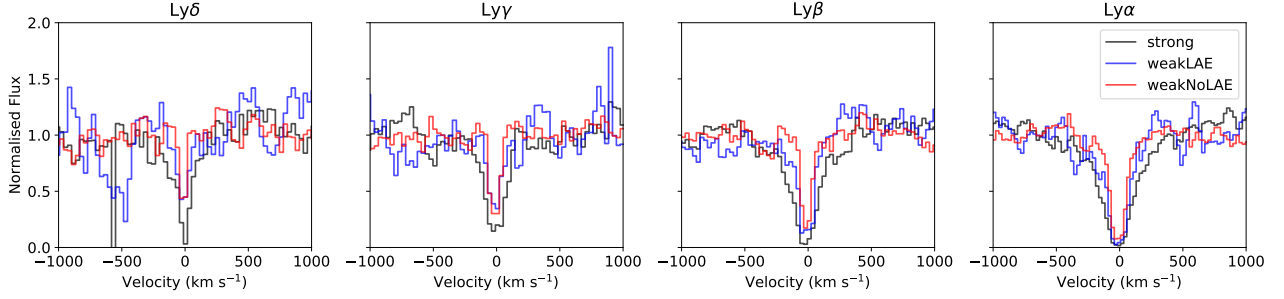


**Figure 17.** Fraction of LAEs aligned (Stacks of Ly $\alpha$ , Ly $\beta$ , Ly $\gamma$  and Ly $\delta$  absorption at the redshift of each C iv system for strong absorbers ( $W_r \geq 0.1 \text{ \AA}$ , black), weak absorbers ( $W_r < 0.1 \text{ \AA}$ , blue) connected to at least one LAE and weak absorbers that are not connected to any galaxies within  $\pm 500 \text{ km s}^{-1}$  (red).

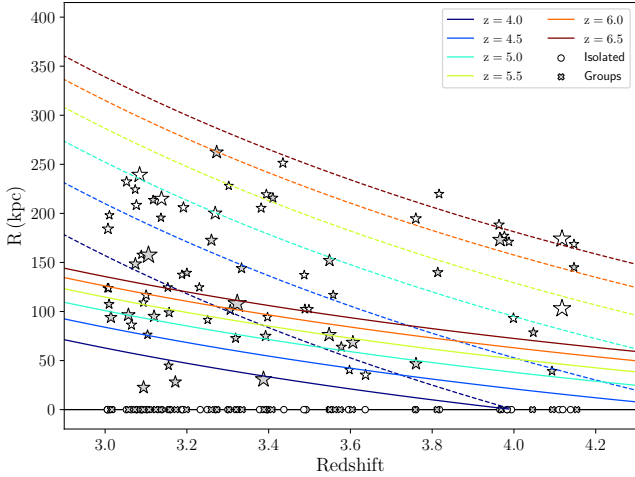


**Figure 18.** Comparison between the distance traveled by outflows ejected during episodes of recent star formation activity (e.g. launched at redshift between  $z = 4$  and  $z = 6.5$  with steps  $\Delta z = 0.5$ ) in the galaxy and the transverse separation between the LAEs (shown at  $R = 0 \text{ kpc}$ ) and the connected C iv absorbers (stars), assuming the outflows travel with average velocities  $\langle v \rangle = 100, 250 \text{ km s}^{-1}$  (solid and dashed lines respectively). We distinguish between C iv associated to isolated galaxies (white-filled markers) and groups (gray-filled markers). The size of the marker is weighted by the rest-frame equivalent width.

absorption-line systems at redshift  $3.0 \lesssim z \lesssim 4.5$ . To extend the analysis of gas-galaxies connection to the lower end of the galaxy mass function, we identified  $> 1000$  LAEs in the MUSE cubes at  $3.0 \lesssim z \lesssim 6.0$ , 292 of which lie in the C iv redshift path and are candidates for an association with the absorbing gas. We found 143 LAEs within a velocity separation  $|\Delta v| \leq 500 \text{ km s}^{-1}$  from C iv absorbers. Given the large size of this sample, we were able to study, for the first time with significant statistics, both the global correlation between LAEs and C iv/Si iv and the properties of the individual associations. The main findings of this work are summarized next.

- We measured, for the first time, the luminosity function of LAEs connected to C iv absorbers. Compared to an updated version of the field luminosity function derived from MAGG, we found a normalization  $\approx 2.4$  higher for LAEs associated with the C iv absorbing gas. This analysis revealed that the LAE number density is sensitive to the proximity to different tracers studied in MAGG and progressively

increases from the field, to the surrounding of C iv gas, strong H i absorbers and central quasars.

- We measured the two-point LAE auto-correlation and LAE-C iv cross-correlation functions and the respective reduced angular auto- and cross- correlation functions. We found a clustering length  $r_0 = 2.07^{+0.23}_{-0.24} \text{ h}^{-1} \text{ cMpc}$  for LAEs and  $r_0 = 1.23^{+0.25}_{-0.27} \text{ h}^{-1} \text{ cMpc}$  for LAE-C iv absorbers, assuming a fixed slope  $\gamma = 1.8$ . Employing the Cauchy-Schwarz relation, we found that a fraction of the C iv absorbers is likely to arise not only in the halo of the LAEs they are connected to, but also from other regions, such as locations in the IGM not connected to galaxies. The LAE-C iv cross-correlation function lies below the cross-correlation function measured between LAEs and optically-thick H i absorbers, indicating a larger contribution from more underdense regions in the C iv case.

- Moving to a galaxy-centered approach (i.e., centering on the galaxies and exploring the surrounding gas distribution) we measure the LAE covering fraction as a tracer of the probability to observe C iv absorbers within  $\pm 500 \text{ km s}^{-1}$  from a galaxy. The covering fraction is observed to decrease with increasing C iv absorption strength and increasing impact parameter up to  $\approx 100 - 150 \text{ kpc}$  from galaxies, at which point it is observed to flatten with elevated values far beyond the virial radius and up to the edge of the FoV. We also found a higher covering fraction for galaxies with luminosity  $\log[L_{\text{Ly}\alpha}/(\text{erg s}^{-1})] > 42.2$  compared to fainter LAEs.

- Among the galaxies connected to the C iv absorbers,  $\approx 30$  per cent are isolated within  $\pm 500 \text{ km s}^{-1}$ , while the remaining  $\approx 70$  per cent are part of a group. The absorbers connected to 1 or at least 2 LAEs show, on average, a rest-frame equivalent width that is a factor  $\approx 1.5$  and  $\approx 4.6$  higher than the median of the full sample, respectively. However, the effect on the gas kinematics is less significant, with only the absorbers connected to more than 1 LAE exhibiting a  $\Delta v_{90}$  that is a factor  $\approx 1.7$  above the median of the full C iv sample. C iv absorbers with larger equivalent width and  $\Delta v_{90}$  tend to be associated with brighter LAEs. The probability to observe a C iv absorber near an LAE is a factor  $\approx 3$  higher around galaxies in groups compared to the isolated ones at any transverse separation. As opposed to what is observed at  $z \lesssim 2$ , the excess of C iv absorption around galaxies in groups is present even if controlling for the properties of isolated galaxies and groups.

- Comparing the statistics of C iv and Si iv absorbers, we found that  $\approx 29$  per cent of the C iv systems show Si iv absorption with the same number of components aligned with the C iv ones. The fraction of Si iv systems' matched to C iv decreases with decreasing equivalent width, and the ratio between the equivalent width of Si iv and C iv is found to be less than unity, as expected from ionization models for densities  $n_{\text{H}} \lesssim 10^{-2} \text{ cm}^{-3}$ . Thus, we conclude that the two

ions, with a similar ionization potential and in the same ionization stage, mostly arise from the same gas phase when detected. This is further supported by the fact that an independent analysis of gas-LAE connection leads to similar results if using either C IV or the Si IV ions as a tracer.

- Despite the large projected distance from LAEs at which C IV absorption is detected (up to the edge of the FoV, corresponding to  $R \approx 250 \text{ kpc} \gtrsim 7 R_{\text{vir}}$  for a dark matter halo  $M_{\text{H}} \approx 10^{11} M_{\odot}$ ), we have found that at least a fraction of the absorbers can be instantaneously enriched by outflows traveling at  $\langle v \rangle \gtrsim 250 \text{ km s}^{-1}$  and launched  $\Delta t \lesssim 750 \text{ Myr}$  before the observations. This makes the CGM and IGM, and in particular an intermediate ionized gas-phase, at least partially linked to the recent star formation activity in galaxies.

- Compared to similar studies about the connection of metals and LBGs, LAEs and (strong) C IV absorbers are less clustered, with a correlation length that is a factor of  $\approx 2$  lower than LBGs at similar redshifts. For both galaxy populations, the ionized gas is extended far beyond the typical virial radius of the halo with a mild (if any) decline in the equivalent width beyond a few hundred kiloparsecs from the galaxy position.

- We found that 43 out of 220 C IV systems are also connected to strong H I absorbers within  $\pm 500 \text{ km s}^{-1}$  in MAGG. We found that these systems show, on average, higher rest-frame equivalent width and more complex kinematics compared to those that are not associated to H I absorption. We did not observe any difference between the properties of the LAEs connected to C IV absorber with or without H I detection, but we found that it is more likely ( $\approx 2\times$ ) for strong H I absorbers to be associated with LAEs than C IV systems.

The combination of this study on gas at intermediate ionization near LAEs and the findings presented in our MAGG IV paper on the link between LAEs and optically-thick H I absorbers, together with literature results, allows to paint a clearer picture for how hydrogen and metals are distributed around  $z \approx 3 - 4$  star-forming galaxies, for the first time extending to lower mass scales ( $M_{\text{H}} \approx 10^{11} M_{\odot}$ ) with a complete and coherent survey. As argued in MAGG IV, data support a model in which star-forming galaxies lie within large-scale structures (i.e., cosmic filaments) and strong H I absorbers are a tracer of the neutral phase both within the CGM of the embedded star-forming galaxies and along the filaments connecting halos. This paper confirms a similar picture for the metals traced by C IV, but only when considering relatively strong absorbers, with  $W \gtrsim 0.1 \text{ \AA}$ , which are more clearly correlated to galaxies and the LLS themselves. For weaker absorbers, our MUSE observations support the idea of a more widespread and homogeneous medium that extends far beyond the CGM of galaxies, also reaching regions away from the densest parts of the filaments where optically-thick H I absorbers are found.

We thus propose a ‘three-component model’ to fit all the principal features uncovered by MAGG near LAEs, which agree with the findings and conclusions by [Muzahid et al. \(2021\)](#). The first component is represented by the CGM of individual systems that gives rise to the strongest H I and C IV absorbers observed at close separation from galaxies and which accounts for the elevated covering factors of hydrogen and metals near LAEs. On these scales, it is more likely that galaxies have a direct impact on the properties of the CGM, as seen for instance in some correlations between emission and absorption properties (e.g., C IV velocity width and absorption strength with  $\text{Ly}\alpha$  luminosity), although as argued in MAGG IV the patchy nature of this gas leads to high scatter in the observed relations. The second component describes the overdense gas along filaments, which accounts for a large fraction of LLSs and for the remaining fraction

of high equivalent-width absorbers. This gas, together with the outer CGM components, is what drives the excess of galaxies located at distances greater than a few times the virial radius and sets the normalization and shape of the luminosity and cross-correlation function for strong H I and C IV systems. The third component is represented by the lower equivalent-width but enriched medium, farther from the denser CGM and the central parts of the filaments connecting galaxies. This medium, which is not easily selected by LLSs, i) accounts for the substantial fraction of C IV for which no LAE counterparts are found; ii) lowers the normalization of the luminosity function and the correlation length of the cross-correlation function; iii) leads to a high covering factor extending to large distances from galaxies; iv) yields a weak dependence of equivalent width with impact parameter. This more diffuse gas is harder to detect with less sensitive tracers like Si IV, which explains the stronger clustering/higher normalization of LAEs near Si IV than C IV (in other words, Si IV is a better tracer of the first two components of this model).

Finally, environment shapes the distribution of gas, particularly the stronger absorbers that seem to be more affected by the presence of groups. Currently, however, it is not particularly clear how environment affects different gas phases (e.g. ionized and neutral components) differently as a function of redshift, and which physical mechanisms are primarily responsible for the observed trends. Refining this picture is the subject of ongoing observational efforts. Observations of other galaxy populations that reside in the same structures are expected to yield comparable results. For instance, LBGs, which are not completely independent from LAEs and relatively more clustered, are too embedded within these structures and carry their own CGM. Hence, most of the trait discussed for LAEs apply to LBGs (as observed), with the exception of a higher clustering of this population.

Biases against the detection of particular systems (e.g., dusty or passive galaxies) are surely present and will inevitably lead to changes in this picture. As argued in MAGG IV, however, the number density of LAEs is sufficiently high that this population becomes a very good tracer of the large-scale structures surrounding galaxies, within which additional undetected populations will reside. We therefore speculate that it is implausible that populations at much lower number density will drastically alter the model put forward here. Future multiwavelength surveys, particularly at infrared/millimetre wavelengths, are required to settle this point. Sustained effort should also be invested in theoretical work to develop a more quantitative model, e.g. using numerical simulations, that can be compared more quantitatively with our observations to test this ‘three-component model’ rigorously.

## ACKNOWLEDGEMENTS

This project has received funding from the European Research Council (ERC) under the European Union’s Horizon 2020 research and innovation programme (grant agreement No 757535) and by Fondazione Cariplo (grant No 2018-2329). SC gratefully acknowledges support from the European Research Council (ERC) under the European Union’s Horizon 2020 research and innovation programme grant agreement No 864361. This work is based on observations collected at the European Organisation for Astronomical Research in the Southern Hemisphere under ESO programme IDs 197.A-0384, 065.O-0299, 067.A-0022, 068.A-0461, 068.A-0492, 068.A-0600, 068.B-0115, 069.A-0613, 071.A-0067, 071.A-0114, 073.A-0071, 073.A-0653, 073.B-0787, 074.A-0306, 075.A-0464, 077.A-0166, 080.A-0482, 083.A-0042, 091.A-0833, 092.A-0011, 093.A-



0575, 094.A-0280, 094.A-0131, 094.A-0585, 095.A-0200, 096.A-0937, 097.A-0089, 099.A-0159, 166.A-0106, 189.A-0424. This work used the DiRAC Data Centric system at Durham University, operated by the Institute for Computational Cosmology on behalf of the STFC DiRAC HPC Facility ([www.dirac.ac.uk](http://www.dirac.ac.uk)). This equipment was funded by BIS National E-infrastructure capital grant ST/K00042X/1, STFC capital grants ST/H008519/1 and ST/K00087X/1, STFC DiRAC Operations grant ST/K003267/1 and Durham University. DiRAC is part of the National E-Infrastructure. This research made use of Astropy (Astropy Collaboration et al. 2013).

## DATA AVAILABILITY

The VLT data used in this work are available from the European Southern Observatory archive (<https://archive.eso.org/>) either as raw data or phase 3 data products. Spectroscopy obtained at the Keck telescopes is available via the Keck Observatory Archive (KOA, <https://www2.keck.hawaii.edu/koa/public/koa.php>). Cubextractor can be obtained upon request by contacting Sebastiano Cantalupo, and other codes used in this paper have been made available at <http://www.michelefumagalli.com/codes.html>.

## ONLINE SUPPORTING INFORMATION

We provide as online material the fits of all the C iv and Si iv absorption lines included in the samples used in this work along with tables listing the properties for each system including redshift, equivalent width and velocity width. We also include the full list of Ly $\alpha$  identified in the MAGG survey at  $SNR > 7$  and the properties of each galaxy including redshift, Ly $\alpha$  luminosity and impact parameter.

## REFERENCES

- Adelberger K. L., Steidel C. C., Shapley A. E., Pettini M., 2003, *ApJ*, **584**, 45
- Adelberger K. L., Shapley A. E., Steidel C. C., Pettini M., Erb D. K., Reddy N. A., 2005, *ApJ*, **629**, 636
- Aguirre A., Hernquist L., Schaye J., Weinberg D. H., Katz N., Gardner J., 2001, *ApJ*, **560**, 599
- Arrigoni Battaia F., Hennawi J. F., Prochaska J. X., Oñorbe J., Farina E. P., Cantalupo S., Lusso E., 2019, *MNRAS*, **482**, 3162
- Astropy Collaboration et al., 2013, *A&A*, **558**, A33
- Bacon R., et al., 2010, in McLean I. S., Ramsay S. K., Takami H., eds, Society of Photo-Optical Instrumentation Engineers (SPIE) Conference Series Vol. 7735, Ground-based and Airborne Instrumentation for Astronomy III. p. 773508, doi:10.1117/12.856027
- Bernstein R., Shectman S. A., Gunnels S. M., Mochnacki S., Athey A. E., 2003, in Iye M., Moorwood A. F. M., eds, Society of Photo-Optical Instrumentation Engineers (SPIE) Conference Series Vol. 4841, Instrument Design and Performance for Optical/Infrared Ground-based Telescopes. pp 1694–1704, doi:10.1117/12.461502
- Bertin E., Arnouts S., 1996, *A&AS*, **117**, 393
- Bielby R. M., et al., 2011, *MNRAS*, **414**, 2
- Bielby R. M., et al., 2016, *MNRAS*, **456**, 4061
- Bielby R., Crighton N. H. M., Fumagalli M., Morris S. L., Stott J. P., Tejos N., Cantalupo S., 2017, *MNRAS*, **468**, 1373
- Bielby R. M., et al., 2019, *MNRAS*, **486**, 21
- Bielby R. M., et al., 2020, *MNRAS*, **493**, 5336
- Bordoloi R., et al., 2011, *ApJ*, **743**, 10
- Bordoloi R., et al., 2014, *ApJ*, **796**, 136
- Borisova E., et al., 2016, *ApJ*, **831**, 39
- Bouché N., Lehnert M. D., Péroux C., 2006, *MNRAS*, **367**, L16
- Burchett J. N., et al., 2016, *ApJ*, **832**, 124
- Cantalupo S., et al., 2019, *MNRAS*, **483**, 5188
- Chen H.-W., Mulchaey J. S., 2009, *ApJ*, **701**, 1219
- Chen H.-W., Lanzetta K. M., Webb J. K., 2001, *ApJ*, **556**, 158
- Chen H.-W., Helsby J. E., Gauthier J.-R., Shectman S. A., Thompson I. B., Tinker J. L., 2010, *ApJ*, **714**, 1521
- Cooksey K. L., Kao M. M., Simcoe R. A., O’Meara J. M., Prochaska J. X., 2013, *ApJ*, **763**, 37
- Crighton N. H. M., et al., 2011, *MNRAS*, **414**, 28
- Crighton N. H. M., Hennawi J. F., Simcoe R. A., Cooksey K. L., Murphy M. T., Fumagalli M., Prochaska J. X., Shanks T., 2015, *MNRAS*, **446**, 18
- D’Odorico V., et al., 2016, *MNRAS*, **463**, 2690
- D’Odorico V., et al., 2022, *MNRAS*, **512**, 2389
- Davis M., Peebles P. J. E., 1983, *ApJ*, **267**, 465
- Dekker H., D’Odorico S., Kaufer A., Delabre B., Kotzlowski H., 2000, in Iye M., Moorwood A. F., eds, Society of Photo-Optical Instrumentation Engineers (SPIE) Conference Series Vol. 4008, Optical and IR Telescope Instrumentation and Detectors. pp 534–545, doi:10.1117/12.395512
- Díaz C. G., Ryan-Weber E. V., Cooke J., Koyama Y., Ouchi M., 2015, *MNRAS*, **448**, 1240
- Díaz C. G., Ryan-Weber E. V., Karman W., Caputi K. I., Salvadori S., Crighton N. H., Ouchi M., Vanzella E., 2021, *MNRAS*, **502**, 2645
- Diener C., et al., 2017, *MNRAS*, **471**, 3186
- Dutta R., et al., 2020, *MNRAS*, **499**, 5022
- Dutta R., et al., 2021, *MNRAS*,
- Ellison S. L., Songaila A., Schaye J., Pettini M., 2000, *AJ*, **120**, 1175
- Felten J. E., 1976, *ApJ*, **207**, 700
- Ferland G. J., et al., 2013, *Rev. Mex. Astron. Astrofis.*, **49**, 137
- Finlator K., Davé R., 2008, *MNRAS*, **385**, 2181
- Finn C. W., et al., 2016, *MNRAS*, **460**, 590
- Fitzpatrick E. L., 1999, *PASP*, **111**, 63
- Fossati M., Fumagalli M., Boselli A., Gavazzi G., Sun M., Wilman D. J., 2016, *MNRAS*, **455**, 2028
- Fossati M., et al., 2019, *MNRAS*, **490**, 1451
- Fossati M., et al., 2021, *MNRAS*, **503**, 3044
- Fumagalli M., O’Meara J. M., Prochaska J. X., 2011, *Science*, **334**, 1245
- Fumagalli M., O’Meara J. M., Prochaska J. X., 2016, *MNRAS*, **455**, 4100
- Fumagalli M., et al., 2017, *MNRAS*, **471**, 3686
- García-Vergara C., Hennawi J. F., Barrientos L. F., Rix H.-W., 2017, *ApJ*, **848**, 7
- García-Vergara C., Hennawi J. F., Barrientos L. F., Arrigoni Battaia F., 2019, *ApJ*, **886**, 79
- Gawiser E., et al., 2007, *ApJ*, **671**, 278
- Hafen Z., et al., 2019, *MNRAS*, **488**, 1248
- Hasan F., et al., 2020, *ApJ*, **904**, 44
- Hasan F., Churchill C. W., Stemock B., Nielsen N. M., Kacprzak G. G., Croom M., Murphy M. T., 2021, arXiv e-prints, p. arXiv:2108.04924
- Hennawi J. F., et al., 2006, *AJ*, **131**, 1
- Herenz E. C., et al., 2019, *A&A*, **621**, A107
- Herrero Alonso Y., et al., 2021, *A&A*, **653**, A136
- Hinton S. R., Davis T. M., Lidman C., Glazebrook K., Lewis G. F., 2016, *Astronomy and Computing*, **15**, 61
- Leclercq F., et al., 2017, *A&A*, **608**, A8
- Liang C. J., Chen H.-W., 2014, *MNRAS*, **445**, 2061
- Lofthouse E. K., et al., 2020, *MNRAS*, **491**, 2057
- Lofthouse E. K., et al., 2022, *MNRAS*,
- Madau P., Dickinson M., 2014, *ARA&A*, **52**, 415
- Maio U., Khochfar S., Johnson J. L., Ciardi B., 2011, *MNRAS*, **414**, 1145
- Marino R. A., et al., 2018, *ApJ*, **859**, 53
- Muzahid S., et al., 2020, *MNRAS*, **496**, 1013
- Muzahid S., et al., 2021, arXiv e-prints, p. arXiv:2105.05260
- Nielsen N. M., Kacprzak G. G., Pointon S. K., Churchill C. W., Murphy M. T., 2018, *ApJ*, **869**, 153
- Oppenheimer B. D., Davé R., 2006, *MNRAS*, **373**, 1265
- Ouchi M., et al., 2010, *ApJ*, **723**, 869
- Patnaik A. R., Browne I. W. A., Walsh D., Chaffee F. H., Foltz C. B., 1992, *MNRAS*, **259**, 1P
- Pettini M., Madau P., Bolte M., Prochaska J. X., Ellison S. L., Fan X., 2003, *ApJ*, **594**, 695

- Pieri M. M., Schaye J., Aguirre A., 2006, *ApJ*, **638**, 45  
 Planck Collaboration et al., 2016, *A&A*, **594**, A13  
 Prochaska J. X., et al., 2019, *ApJS*, **243**, 24  
 Rafelski M., Neeleman M., Fumagalli M., Wolfe A. M., Prochaska J. X., 2014, *ApJ*, **782**, L29  
 Rakic O., Schaye J., Steidel C. C., Rudie G. C., 2011, *MNRAS*, **414**, 3265  
 Robert P. F., Murphy M. T., O'Meara J. M., Crighton N. H. M., Fumagalli M., 2019, *MNRAS*, **483**, 2736  
 Rubin K. H. R., Diamond-Stanic A. M., Coil A. L., Crighton N. H. M., Moustakas J., 2018, *ApJ*, **853**, 95  
 Rudie G. C., et al., 2012, *ApJ*, **750**, 67  
 Rudie G. C., Steidel C. C., Pettini M., Trainor R. F., Strom A. L., Hummels C. B., Reddy N. A., Shapley A. E., 2019, *ApJ*, **885**, 61  
 Scannapieco E., Ferrara A., Madau P., 2002, *ApJ*, **574**, 590  
 Schaye J., Aguirre A., Kim T.-S., Theuns T., Rauch M., Sargent W. L. W., 2003, *ApJ*, **596**, 768  
 Schechter P., 1976, *ApJ*, **203**, 297  
 Schlafly E. F., Finkbeiner D. P., 2011, *ApJ*, **737**, 103  
 Schmidt M., 1968, *ApJ*, **151**, 393  
 Schneider R., Ferrara A., Natarajan P., Omukai K., 2002, *ApJ*, **571**, 30  
 Schroetter I., et al., 2021, *MNRAS*, **506**, 1355  
 Sheinis A. I., Bolte M., Epps H. W., Kibrick R. I., Miller J. S., Radovan M. V., Bigelow B. C., Sutin B. M., 2002, *PASP*, **114**, 851  
 Shen S., Madau P., Guedes J., Mayer L., Prochaska J. X., Wadsley J., 2013, *ApJ*, **765**, 89  
 Simcoe R. A., Sargent W. L. W., Rauch M., 2004, *ApJ*, **606**, 92  
 Simcoe R. A., et al., 2011, *ApJ*, **743**, 21  
 Songaila A., 2005, *AJ*, **130**, 1996  
 Steidel C. C., Erb D. K., Shapley A. E., Pettini M., Reddy N., Bogosavljević M., Rudie G. C., Rakic O., 2010, *ApJ*, **717**, 289  
 Steidel C. C., Bogosavljević M., Shapley A. E., Kollmeier J. A., Reddy N. A., Erb D. K., Pettini M., 2011, *ApJ*, **736**, 160  
 Stott J. P., et al., 2020, *MNRAS*, **497**, 3083  
 Tejos N., et al., 2014, *MNRAS*, **437**, 2017  
 Trainor R. F., Steidel C. C., 2012, *ApJ*, **752**, 39  
 Tremonti C. A., et al., 2004, *ApJ*, **613**, 898  
 Turner M. L., Schaye J., Steidel C. C., Rudie G. C., Strom A. L., 2014, *MNRAS*, **445**, 794  
 Verhamme A., et al., 2018, *MNRAS*, **478**, L60  
 Vernet J., et al., 2011, *A&A*, **536**, A105  
 Vogt S. S., et al., 1994, in Crawford D. L., Craine E. R., eds, Society of Photo-Optical Instrumentation Engineers (SPIE) Conference Series Vol. 2198, Instrumentation in Astronomy VIII. p. 362, doi:10.1117/12.176725  
 Weibacher P. M., Streicher O., Urrutia T., Pécontal-Rousset A., Jarno A., Bacon R., 2014, in Manset N., Forshay P., eds, Astronomical Society of the Pacific Conference Series Vol. 485, Astronomical Data Analysis Software and Systems XXIII. p. 451 (arXiv:1507.00034)  
 Welsh L., Cooke R., Fumagalli M., 2019, *MNRAS*, **487**, 3363  
 Wise J. H., Turk M. J., Norman M. L., Abel T., 2012, *ApJ*, **745**, 50  
 Wisotzki L., et al., 2016, *A&A*, **587**, A98  
 de La Vieuville G., et al., 2019, *A&A*, **628**, A3

## APPENDIX A: THEORETICAL COMPARISON BETWEEN C iv AND Si iv ABSORBERS AS TRACERS OF THE IONIZED GAS

We complemented the comparison between C iv and Si iv absorbers shown in Section 4.6 with a more theoretical approach: indeed, one way to test the assumption that C iv and Si iv absorbers trace the same gas phase is to examine whether absorbers arising at the same redshift are composed of the same number of components that are aligned in redshift. By searching for Si iv lines detected within  $|\Delta v| \leq 150 \text{ km s}^{-1}$  from a C iv absorber, we identify 63 matched systems (corresponding to the  $\approx 29\%$  of the full C iv sample, and  $\approx 58\%$  of the Si iv systems). We model the absorption of these profiles by fitting the lines with the MC-ALF code, following the method

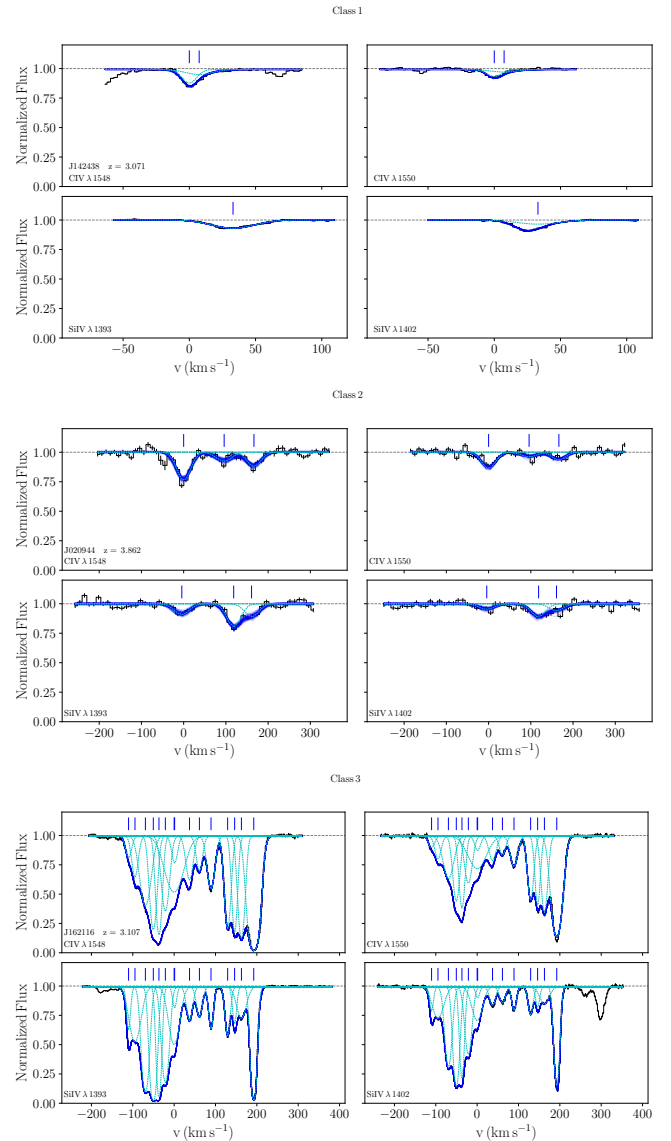


**Figure A1.** Examples of C iv and Si iv systems matched within  $\pm 150 \text{ km s}^{-1}$  in velocity space and classified according to the number and the alignment of Voigt components (class 1-3 from top to bottom, see text for details).

presented in Rudie et al. (2019) to identify the number of aligned components. Based on the alignment of each component, we classify the matched systems into three classes (see Figure A1 for examples): i) systems that are clearly misaligned, suggesting that C iv and Si iv absorbers are not tracers of the same gas structure. This class contains  $\approx 10\%$  (6/63) of the matched systems; ii) systems in which the strong components are offset or only partially aligned, i.e. separated by  $\Delta v \gtrsim 10 - 20 \text{ km s}^{-1}$  in velocity space ( $\approx 13\%$ , 8/63, of the matched systems belong to this class, plus the 157 C iv systems that do not show a Si iv counterpart); iii) systems with the same number of components that are clearly aligned (this class contains  $\approx 77\%$  (49/63) of the matched systems). The rate of matches we observe is qualitatively in line with the recent statistical measures from D’Odorico et al. (2022). With a sample of over 600 Si iv absorbers detected in 147 quasar sightlines at redshift  $2.1 \lesssim z_{\text{QSO}} \lesssim 6.5$ , they studied the column density distribution function and found that the abundance of C iv and Si iv ions trace each other across a large red-

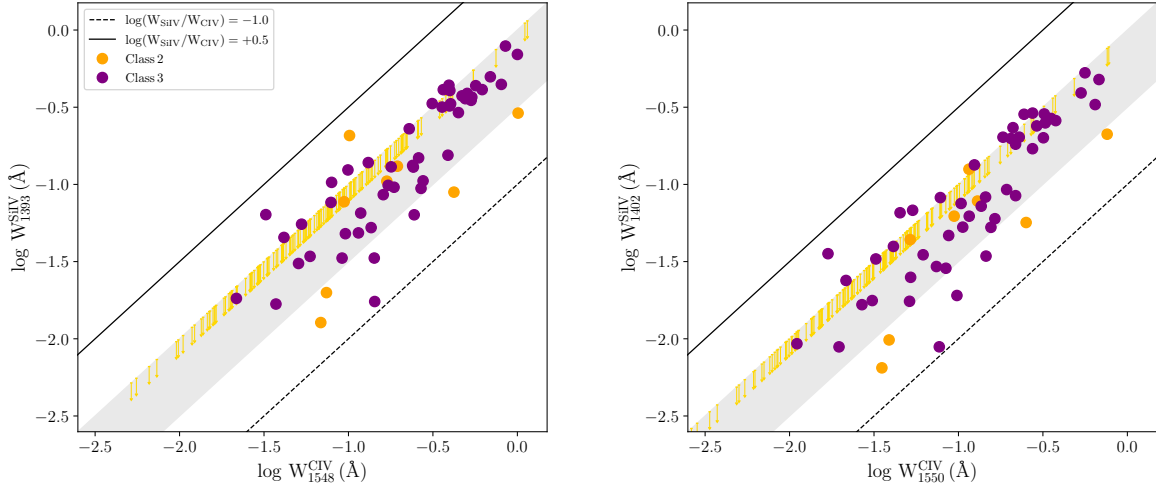


**Figure A2.** Comparison between the rest-frame equivalent width of Si iv absorbers,  $W_{\text{SiIV}}$ , as a function of the equivalent width of the matched C iv system,  $W_{\text{CIV}}$ . Aligned absorbers from class 3 (purple) are distinguished from class 2 systems (orange). The predictions from CLOUDY ionization models (see text for details) are shown as solid and dashed lines, marking  $\log(W_{\text{SiIV}}/W_{\text{CIV}}) = +0.5$  and  $\log(W_{\text{SiIV}}/W_{\text{CIV}}) = -1.0$  respectively. The shaded region highlights the range occupied by the  $\approx 2/3$  of the distribution of aligned detections, corresponding to  $-0.5 < \log(W_{\text{SiIV}}/W_{\text{CIV}}) < 0$ . Arrows show upper limits corresponding to  $\log W_{\text{SiIV}} \leq \log W_{\text{CIV}}$  for Si iv non detections.

shift range. However, the Si iv number density per unit redshift path is a factor  $\approx 2$  lower than the C iv absorbers at any redshift. This difference implies a fraction of  $\lesssim 50\%$  of the C iv systems with a detected Si iv counterpart, as we observe.

Having identified the aligned components in each transition, we measure the rest-frame equivalent width for class 2 and 3 systems and recover how the Si iv equivalent width,  $W_{\text{SiIV}}$ , scales as a function of the equivalent width of the matched C iv absorber,  $W_{\text{CIV}}$ . This estimate allow us to better understand the nature of the class 2 systems and test whether the partial alignment or the offset of the strong components is a sign that systems are not tracing the same gas structures. To complete the picture, we also compare the observed trend with the theoretical predictions from a set of ionization models using CLOUDY (Ferland et al. 2013). The results from the observations are shown in Figure A2, where the shaded region and its limits are derived from CLOUDY, using the “minimal grid” from Fumagalli et al. (2016). Assuming the metallicity to be fixed at  $\log(Z/Z_{\odot}) = -2.0$ , we show the mean equivalent width ratio over the redshift range  $z = 3.0 - 4.5$  as a function of the neutral hydrogen column density and the density in the left-panel of Figure A3.

As it can be seen from this grid, the equivalent width ratio is  $\log(W_{\text{SiIV}}/W_{\text{CIV}}) \approx -1.0$  at densities  $\log(n_{\text{H}}/\text{cm}^{-3}) \lesssim -4$  (for reference, the mean cosmic density at redshift  $z \sim 3$  is  $\log(n_{\text{H}}/\text{cm}^{-3}) \approx -5.0$ ), increases to  $\log(W_{\text{SiIV}}/W_{\text{CIV}}) \approx 0$  at  $-4 \lesssim \log(n_{\text{H}}/\text{cm}^{-3}) \lesssim -2.5$  and about  $\log(W_{\text{SiIV}}/W_{\text{CIV}}) \approx 0.5$  at higher densities  $\log(n_{\text{H}}/\text{cm}^{-3}) \gtrsim -2.5$ . Thus, for common CGM/IGM densities of  $\log(n_{\text{H}}/\text{cm}^{-3}) \lesssim -2.5$ , it is reasonable to expect that only a fraction of C iv absorbers is detected also in Si iv, which will typically appear as weaker line. Indeed, the right panel of Figure A3, which shows the distribution of the C iv-Si iv detections as a function of the C iv rest frame equivalent width, provides clear evidence that detection of Si iv counterparts decline with decreasing strength of the C iv absorbers, significantly dropping close to the sensitivity limits of our spectra at  $W_{\text{SiIV}} \lesssim 10^{-2} \text{ \AA}$ .

Figure A2 provides evidence that our observations of the aligned components are consistent with the ionization models predictions since the class 3 systems are scattered between  $-1.0 \lesssim$

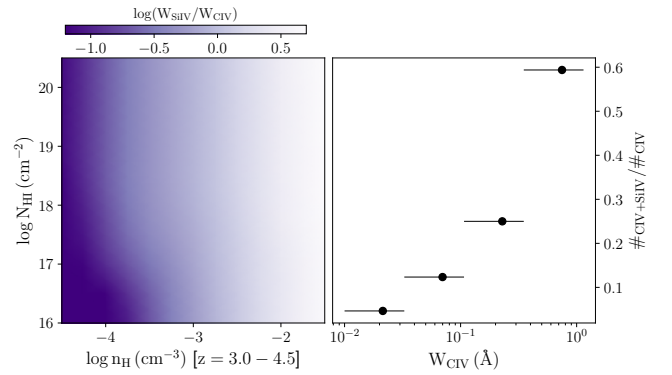


**Figure A3.** Left panel: mean equivalent width ratio over the redshift range  $z = 3.0 - 4.5$  as predicted from a grid of ionization models in the  $\log N_{\text{HI}} - \log n_{\text{H}}$  plane. The metallicity is fixed to  $\log(Z/Z_{\odot}) = -2.0$ . Right panel: distribution of the matching C iv-Si iv detections, normalized to the number of C iv systems in each  $W_{\text{CIV}}$  interval, as a function of the C iv rest frame equivalent width. Horizontal error-bars account for the width of each bin.

$\log(W_{\text{SiIV}}/W_{\text{CIV}}) \lesssim 0.5$ . We observe most of the matched systems at  $\log W_{\text{SiIV}} \lesssim \log W_{\text{CIV}}$ , with only few Si iv absorbers stronger than their C iv counterpart. About 38% (3/8) of the partially-aligned systems (class 2) follow the trend observed for the aligned systems, while the remaining sample is scattered toward a lower ratio  $\log(W_{\text{SiIV}}/W_{\text{CIV}}) \approx -1.0$  pinpointing to the presence of C iv absorption that is significantly stronger or with a higher number of components compared to the Si iv counterpart. We show upper limits (gold arrows in Figure A2) for the C iv absorbers without Si iv counterpart within  $\pm 150 \text{ km s}^{-1}$ , assuming  $\log W_{\text{SiIV}} \leq \log W_{\text{CIV}}$ . As expected from the analysis above, we observe that a large fraction of non-detections corresponds to weak C iv systems with  $\log(W_{\text{CIV}}/\text{\AA}) \lesssim -1.5$ , with only few strong absorbers ( $\log(W_{\text{CIV}}/\text{\AA}) \gtrsim -0.5$ ) lacking associations. The last result support the hypothesis that weak C iv systems would be associated to aligned Si iv absorbers below the detection limit of the survey. In the end, this analysis supports the idea

that C IV and Si IV absorbers are, to first approximation, two tracers of the same gas phase and are expected to lead to comparable results if used to trace an intermediate ionized phase of the CGM and IGM near LAEs.

This paper has been typeset from a  $\text{\TeX}/\text{\LaTeX}$  file prepared by the author.